

NASA Contractor Report 3627

NASA
CR
3627
c. 1

Stability and Control of the Gossamer Human-Powered Aircraft by Analysis and Flight Test

Henry R. Jex and David G. Mitchell

CONTRACT NAS4-2705
OCTOBER 1982

TECH LIBRARY KAFB, NM
0062184
0062184
TECH LIBRARY KAFB, NM

NASA





NASA Contractor Report 3627

Stability and Control of the Gossamer Human-Powered Aircraft by Analysis and Flight Test

Henry R. Jex and David G. Mitchell
Systems Technology, Inc.
Hawthorne, California

Prepared for
Dryden Flight Research Facility
under Contract NAS4-2705



National Aeronautics
and Space Administration

Scientific and Technical
Information Branch

1982

NOTICE

This report was prepared to document work sponsored by the United States Government. Neither the United States nor its agent, the National Aeronautics and Space Administration, nor any Federal employees, nor any of their contractors, subcontractors or their employees, makes any warranty, expressed or implied, or assumes any legal liability or responsibility for the accuracy, completeness, or usefulness of any information, apparatus, product or process disclosed, or represents that its use would not infringe privately owned rights.

PREFACE

This project was a joint effort among three groups: AeroVironment Inc. (whose staff represented the principal developers of the Gossamer aircraft), Systems Technology, Inc. (who did much of the original stability and control work on them), and NASA Dryden Flight Research Center (who supported the flight test work).

The work reported here was performed during two periods: the flight tests from January through May 1980, and data analyses from April through December 1981. Both were under subcontract from AeroVironment Inc., in turn under Contract NAS4-2705 from the NASA Dryden Flight Research Center. The NASA Contract Technical Monitor was Mr. Dale Reed, while the contractor's Principal Investigator and Technical Director was Dr. Paul B. MacCready. Systems Technology, Inc.'s roles were to analyze the stability and control of the Gossamer Albatross II, help plan certain flight tests having to do with the dynamics of the vehicle, participate in the operation of relevant flight tests, reduce the dynamic response data, and compare it with the analyses to assess the adequacy of the state-of-the-art in stability and control analyses for this unconventional class of aircraft.

TABLE OF CONTENTS

	<u>Page</u>
PREFACE	iii
TABLE OF CONTENTS	v
LIST OF FIGURES	vii
LIST OF TABLES	ix
1. INTRODUCTION	1-1
1.1 Motivation	1-1
1.2 Approach	1-2
2. DESCRIPTION OF TESTS	2-1
2.1 Equipment	2-1
2.1.1 Gossamer Albatross II Aircraft	2-1
2.1.2 Flight Test Instrumentation	2-6
2.2 Procedures	2-8
2.3 Data Reduction	2-10
3. RESULTS AND DISCUSSIONS	3-1
3.1 Longitudinal	3-1
3.1.1 Time History	3-1
3.1.2 Pitch Rate Response	3-1
3.1.3 Normal Acceleration Response	3-5
3.1.4 Airspeed Response	3-7
3.2 Lateral-Directional Data	3-7
3.2.1 Responses to Wing Warping	3-7
3.2.2 Responses to Canard Rudder Tilting	3-14
3.2.3 Yaw Rate Response to Canard Tilt	3-17
3.2.4 Roll Rate Response to Canard Tilt	3-17
4. CONCLUSIONS AND RECOMMENDATIONS	4-1
5. REFERENCES	5-1

APPENDIX - Dynamic Stability and Control Analysis

LIST OF FIGURES

<u>Figure</u>	<u>Description</u>	<u>Page</u>
2-1a	Three-view of Gossamer Condor	2-2
2-1b	Three-view of the Gossamer Albatross	2-3
2-2	Estimated Albatross-II drag, power and aerodynamic trim conditions versus airspeed	2-5
2-3	Gossamer Albatross flight test instrumentation	2-7
2-4	The Gossamer Albatross-II in flight during a typical test at NASA Dryden Flight Research Center	2-11
3-1	Time history of Flight 4 for longitudinal data	3-2
3-2	Pitch rate response to canard elevator frequency sweep	3-3
3-3	Normal acceleration response to canard elevator frequency sweep	3-6
3-4	Sensed airspeed response to canard elevator	3-8
3-5	Time history of Flight 15 for lateral-directional data	3-9
3-6	Roll rate response to wing warp frequency sweep	3-11
3-7	Roll rate response to wing warp frequency sweep	3-12
3-8	Summary of best data for roll rate response to wing warp	3-13
3-9	Yaw rate response to wing warp	3-15
3-10	Time history of Flight 6 for canard tilt data	3-16
3-11	Yaw rate response to canard tilt frequency sweep; Flight 6	3-18
3-12	Yaw rate response to canard tilt frequency sweep	3-19
3-13	Summary of best data for yaw rate response to canard tilt	3-20
3-14	Roll rate response to canard tilt frequency sweep; Flight 6	3-22
3-15	Roll rate response to canard tilt	3-23
3-16	Summary of best data for roll rate response to canard tilt	3-24

LIST OF FIGURES (continued).

<u>Figure</u>	<u>Description</u>	<u>Page</u>
A-1	Transient response of Gossamer Condor to a leftward wing warp	A-26
A-2	Transient response of Gossamer Condor to a rightward canard tilt	A-27
A-3	Time response of a closed-loop turn entry for the Gossamer Condor	A-28

LIST OF TABLES

<u>Table</u>	<u>Description</u>	<u>Page</u>
A-1a	Key aerodynamic dimensions for Gossamer Condor	A-12
A-1b	Key aerodynamic dimensions for Gossamer Albatross II	A-13
A-2a	Inertial parameters for Gossamer Condor	A-14
A-2b	Inertial parameters for Gossamer Albatross	A-15
A-3	Trim conditions and nondimensional aerodynamic derivatives at cruise	A-16
A-4	Longitudinal equations of motion	A-18
A-5	Longitudinal transfer functions	A-19
A-6	Lateral-directional equations of motion	A-20
A-7	Lateral-directional transfer functions	A-23

1. INTRODUCTION

1.1 Motivation

The Gossamer series of man-powered aircraft* designed by Dr. Paul B. MacCready and his associates, represent a new class of ultralight designs which are characterized by low power requirements (less than 0.5 horsepower, or 373 watts); very low wing loadings (under $.5 \text{ lb/ft}^2$ or 24 N/m^2); flight at low airspeeds (around 10 to 15 miles per hour or 4.5 to 6.7 m/s); unusual configurations (canard elevator, pusher propeller); advanced composite plastic structure (carbon-filament-reinforced epoxy tubing); and novel control techniques (tilting canard rudder) [Refs. 1, 2].

In the Gossamer designs, good stability and handling were secondary to obtaining the absolute minimum-power design. As a result of this minimum-power design, a number of stability and control problems were uncovered and solved during the Gossamer Condor's development, through a combination of discovery, trial-and-error, and analysis [Refs. 3, 4]. The Gossamer Albatross was a much-refined version of the basic Gossamer Condor configuration.

The basic technology has proven applicable to solar-cell electric-powered aircraft, where low power is a necessity; the AeroVironment Gossamer Penguin was the first piloted aircraft to fly solely on the power of sunlight; and the Solar Challenger was the first solar-electric aircraft developed to perform long, high altitude flights, flying from Paris to England in 1980 [Ref. 5].

These developments open the possibilities of flights of essentially unlimited duration by solar-electric aircraft of similar design at higher altitudes, and could, in one extreme, become a "poor man's satellite" for relaying information via line-of-sight transmissions.

To investigate this ultralight aircraft technology, NASA sponsored a series of very brief performance and stability and control flight tests of of the Gossamer Albatross II at

*In 1977 the Gossamer Condor was the first man-powered aircraft to fly the Kremer course (a figure-eight around two pylons, one-half mile apart and clear a 10-foot (3 m) barrier). The Gossamer Albatross I was the first man-powered aircraft to fly the English Channel, taking 2.8 hours from Folkestone to Cape Gris Nez, in 1979.

the Dryden Flight Research Center (Edwards Air Force Base, California) in the spring of 1980. The primary objectives of the flight tests were, to the extent possible, to measure:

- (1) the performance properties, such as lift-to-drag, power required, propeller efficiency, and trim speed effects.
- (2) the dynamic response properties to various control inputs to verify the computed stability and control characteristics.

Systems Technology, Inc.'s role focused on the second objective, and only the stability and control tests are presented herein. The results should be of value in extrapolating such designs to flight at much higher altitudes and in designing suitable automatic and manual control systems for this class of aircraft in the future.

1.2 Approach

Both analysis and flight tests are employed to reveal and permit understanding of the stability and control characteristics of these ultralight designs. Most of the analysis evolved during the development of the Gossamer Condor, as best chronicled by Grosser [Ref. 4] and technically described by Lissaman et al. [Ref. 2]. It includes conventional stability and control derivative and dynamic analyses [Refs. 6, 7], with some additional terms required to account for important "apparent mass" effects (described later herein) and for the control effectiveness of the wing warp and tilted canard rudder controls. These Condor analyses are included here in the Appendix, in which comparable computations have been added for the Albatross II at two speeds: a low (minimum power) speed, and a higher speed more characteristic of the highest speed encountered in the flight tests.

The original analyses in Lissaman et al. [Ref. 2] included a closed-loop pilot/vehicle flight control analysis using a very simple pilot model. These have been omitted here so as to focus solely on the Gossamer aircraft stability and control dynamics.

As shown in the Appendix, the dynamic stability modes of the Gossamer-type aircraft are very highly damped with no overshoots or oscillations, and a few modes have

comparable frequencies or time constants. These facts make it difficult to identify the dynamics by conventional transient response techniques. We opted to use a frequency domain approach, wherein control deflection frequency sweeps are used to obtain the frequency domain, nonlinear "describing function," which approximates the system's transfer function for small amplitudes about the trim condition [see Refs. 7 and 8, for details of the techniques]. These measured describing functions are then compared with the transfer functions computed in the Appendix.

Further data analysis to break down the measured describing functions into aerodynamic coefficients in the equations of motion was not attempted here for two reasons:

- (1) It is not yet certain whether or not the modified rigid equations are correct (i.e., at such low speeds -- where the aircraft takes six seconds to travel one span's distance -- the use of apparent mass terms may be only a portion of the general unsteady aerodynamic effects of importance). Thus, any attempt to fit the coefficients to the data by either time- or frequency-domain methods would give misleading results.
- (2) The program budget was too limited to undertake the more massive analyses required to identify both the correct equations and their coefficients.

The availability (on loan) of a miniaturized 22-channel telemetry unit and many sensors (described in Section 2.1) made possible the recording of many motion and performance variables of interest, but the short time slot of its availability set the schedule and pace of testing. This, and the limited budget, precluded the iterative test-analysis/test-analysis cycle which is desirable in such exploratory flight testing. Further, the limited availability of the Albatross II required testing under winter desert conditions, where calm air is rarely found.

To relieve the pilot from having to both power the aircraft and perform test maneuvers, and to measure the performance variables, a battery-powered electric motor was fitted to power the propeller (see Section 2.1). For some performance runs, the propeller was removed and a towline with a force transducer was attached to directly

measure the thrust. As things turned out, the motor calibrations of voltage and current were hard to match to the propeller power absorbed, and the tow forces proved to be very erratic due to small wind fluctuations, apparent-mass effects, and vehicle accelerations, so the performance data have not yet been analyzed in detail.

Before going on to describe the tests, and because the detailed analyses and descriptions of the dynamic modes are in the Appendix, it is pertinent to summarize here the unconventional aerodynamic stability and control effects which were investigated.

The analyses in the Appendix show that the Gossamer aircraft has negligible static stability but very high damping in pitch, roll, and sway. Thus, pitch attitude control by the canard is like a pure rate-controlled element (pitch rate proportional to elevator deflection), not unlike that of an automobile at low speed (wherein yaw rate is proportional to steering wheel deflection). A key question was to verify this prediction and the approximate transfer functions worked out in Lissaman et al. [Ref. 2] and the Appendix; it implies benign handling qualities in pitch despite the zero static stability. Excellent data were obtained relating to these questions.

The control of height by power variations was shown [Ref. 2] to be relatively simple, and it was of interest in these tests to verify the complex nonphugoid-like dynamics involved. However, the planned thrust variation runs were not obtained in the time available, so this question remains to be answered.

The lateral control of man-powered aircraft has always been a major problem [Ref. 9]. In fact, the Gossamer Condor was the first design in over 15 years of numerous attempts to be easily turned around the 1.3-mile, figure-eight course required by the Kremer Prize rules [Ref. 4]. There were two fundamental lateral control difficulties, which were puzzling when first encountered [Refs. 4, 14], but were clearly revealed by the early analyses and solved concurrently with them:

- (1) The turn radius is not large compared to the span, so the outer wing tip travels much faster than the inner tip (roughly, a 40% difference in the Gossamer aircraft case). This leads (for wings operating at high lift coefficient) to a large lift gradient across the span, and the resulting rolling moment towards

the center of the turn is very difficult to trim out with conventional ailerons or spoilers. This was solved by warping the entire wing opposite to the turn, thereby restoring an even lift distribution (having low drag), and a favorable yawing moment effect, as well. The tilting canard rudder provides the necessary yawing control moments for coordinating the turn by tilting its large trim lift vector.

- (2) The Gossamer aircraft have exceptionally light wing loadings (around $W/S = .4$ to $.5 \text{ lb/ft}^2$ or 19 to 24 N/m^2) which are of the same order as the "apparent-mass" (weight) of air affected by wing vertical accelerations. (The latter is the weight in a cylinder of air having the wing chord as diameter.) This means that it is very difficult to start a wing tip moving downwards as is required for good roll control, while it is much easier to cause the wing to start yawing. This problem is overcome in the Gossamer designs by using the canard rudder to cause yaw rates, whereby the differential airspeed across the span provides a powerful rolling moment for dynamic roll control [see Ref. 2 and Appendix]. Trim roll control is supplied by steady sideslip in combination with the dihedral effect of the slightly swept wings.

The verification of these principles and dynamics was of paramount importance in these tests, and good data relating to them were obtained.

2. DESCRIPTION OF TESTS

2.1 Equipment

2.1.1 Gossamer Albatross II Aircraft

Although the analyses in the Appendix are given for both the Gossamer Condor and Gossamer Albatross aircraft, only the Albatross was flight-tested. Approximate three-views of each aircraft are given in Figures 2-1a and 2-1b, taken from MacCready and Moulton [Refs. 1, 11], respectively. Details of the Albatross design, construction, and control systems are given in Burke [Ref. 3] and Moulton [Ref. 11] and will not be repeated here.

The basic design concept is that of a minimal power-required aircraft having minimal wetted area to reduce parasite drag, a long span to reduce induced drag, wire-braced composite structure to minimize the empty weight to about one-half of the pilot, a universally-mounted canard surface for pitch and yaw control (via tilting its always-upward trim lift vector), a pusher propeller to simplify the drive train and provide some additional yaw stability, wing-warp balancing trim for steady turning, and an optimum fineness-ratio thick fin to contain the pilot in an upright position for optimum pedalling and provide some side force capability. The tested Albatross II was nearly identical to the Channel crossing Albatross I, with the following exceptions:

<u>Albatross</u>	<u>I - Channel Crossing</u>	<u>II - Flight Tests</u> ⁶
Wing Span	93.8 ft (28.6 m)	96.0 ft (29.3 m)
Wing Area	474 ft ² (44.0 m ²)	488 ft ² (45.3 m ²)
Gross Weight (ref)	215.4 lb (97.7 kgw)*	222.0 lb (101.7 kgw)
Wing Loading	.454 lb/ft ² (21.7 N/m ²)	.455 lb/ft ² (21.8 N/m ²)
Power Plant	Human (Bryan Allen)	Electric Motor

*Basic computations herein were made in conventional U.S. customary units (ft, lb, slugs) and then converted to approximate S.I. units (m, N, kg). In accordance with common usage, however, metric weights are given as kgw (1 kgw = weight of 1 kg mass at sea level = 9.807 N = .4536 lb).

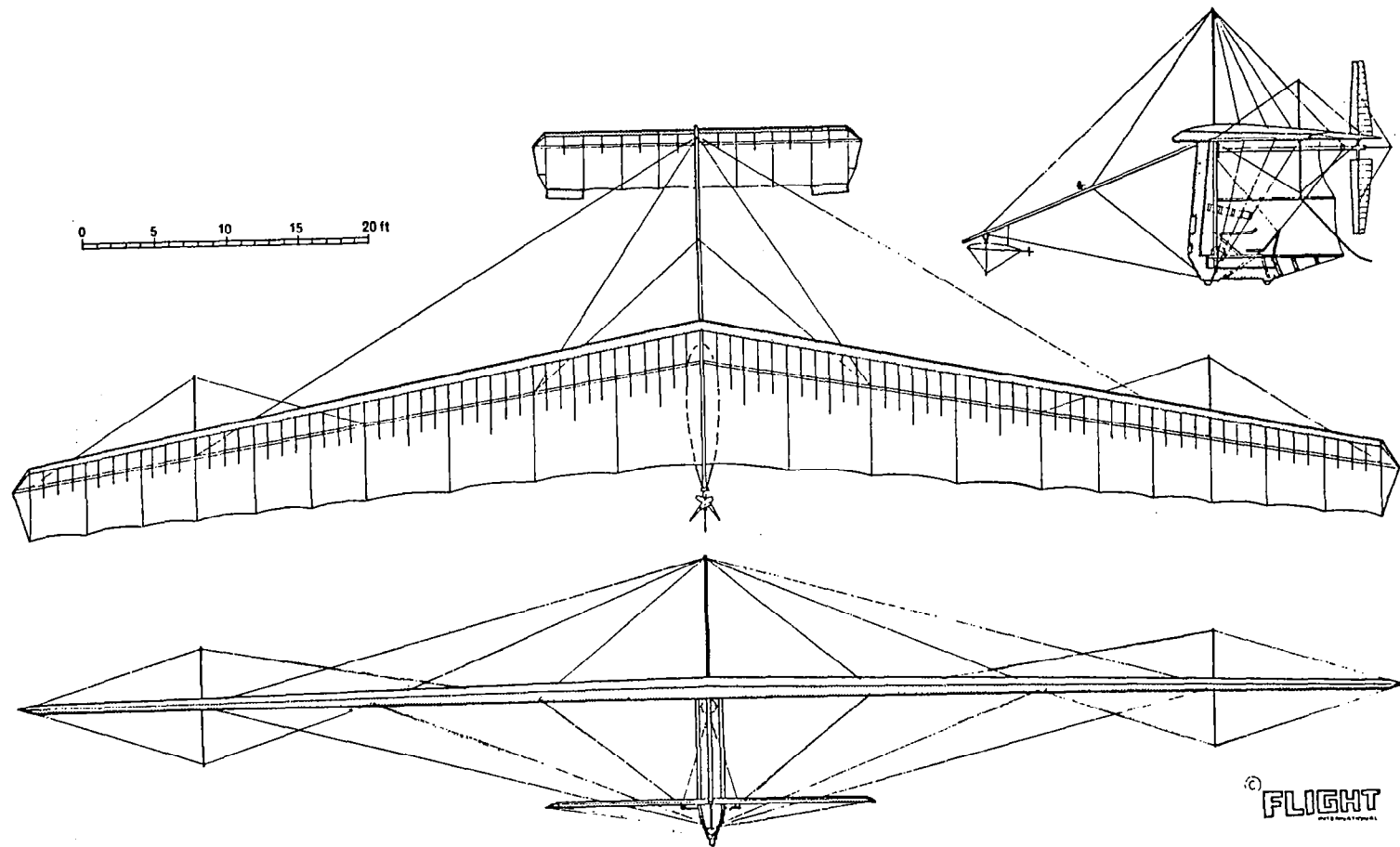


Figure 2-1a. Three-View of Gossamer Condor.

FLIGHT International, 28 July 1979

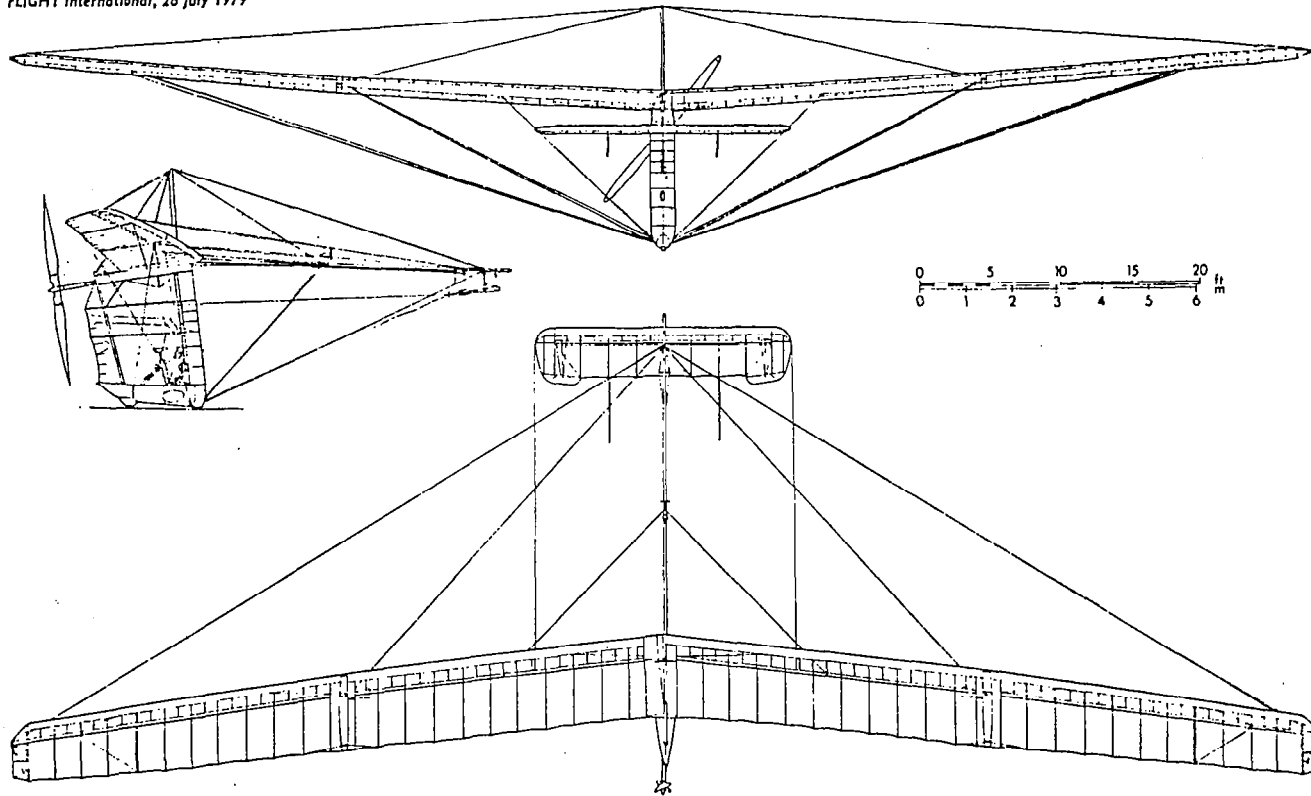


Figure 2-1b. Three-View of Gossamer Albatross.

The differences are so small that the flight test results can be applied directly to the channel-crossing aircraft.

Complete tables of the important aerodynamic dimensions for the Gossamer Condor and Gossamer Albatross II are given in the Appendix.

As noted earlier, an electric motor was installed to relieve the pilot of the chore of providing power, in addition to performing the flight-test maneuvers. Astro-Flight, Inc. (Venice, California) provided a power system incorporating two standard Astro 25 electric motors to give about .34 hp (250 watts). The motors operated at about 12,500 rpm, and were coupled to the propeller drive shaft by belt-belt-chain drive with a 125:1 reduction, giving a propeller speed of approximately 100 rpm. Power was supplied by a 28-volt rechargeable NiCad battery having an approximately 112-Whr capacity at operating conditions. A separate battery powered the telemetry unit described below.

Based on a detailed drag breakdown and likely airfoil properties, estimates of the performance and trim conditions versus airspeed were made for the Albatross II to help select trim conditions; the results are summarized in Figure 2-2. While these computations must be considered approximate, several points are worth noting:

- (1) The flight-tested speed range of 14 to 16 mph (about 7 m/s) spans the minimum drag speed and is just above the minimum power speed. This lends some credibility to the estimates because the tests were flown near minimum power conditions.
- (2) The wing and overall trim lift coefficients are roughly equal at values near $C_{L^w} = 0.8$ to 1.0; optimum conditions for which this Lissaman 7669 airfoil was designed (it is a Stratford recovery-type; see Ref. 13).
- (3) Near the minimum power speed, the canard elevator carries approximately 8% of the total lift, resulting in a lift coefficient (based on its own area) of about $C_{L^c} = .4$ to .5. Since a large canard lift force is necessary for adequate yaw control (via tilting the canard), the present flight test speeds are about the highest which could be adequately controlled.

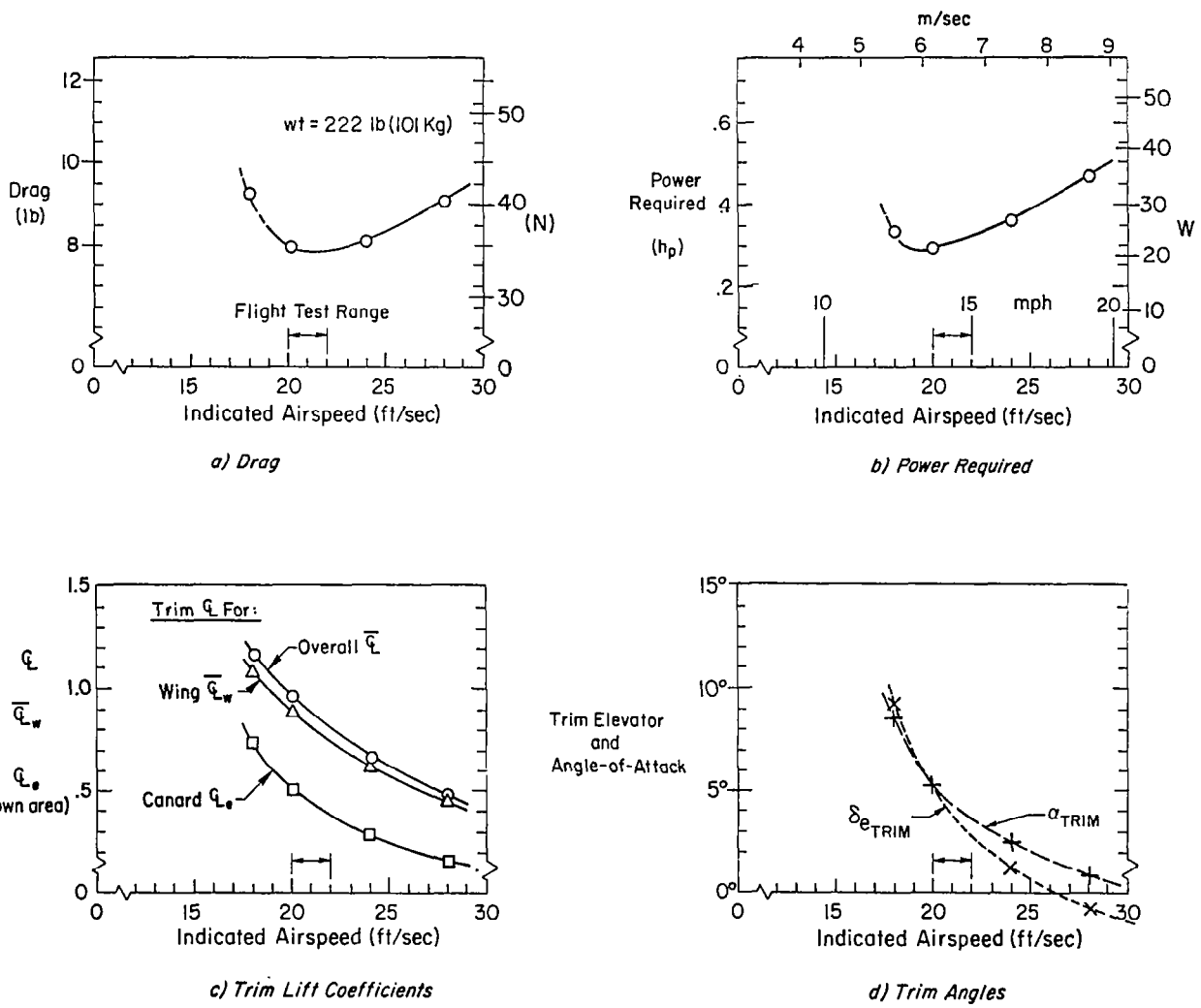


Figure 2-2. Estimated Albatross-II Drag, Power and Aerodynamic Trim Conditions versus Airspeed.

These trim computations verify an important observation made with respect to the Gossamer design and tilt-canard yaw control: it is intrinsically well suited only to a very narrow range of operating points between the highest C_L for low drag and the lowest canard trim C_L (here, between about 19 to 23 ft/sec (13 to 16 mph, or 6 to 7 m/s)).

2.1.2 Flight Test Instrumentation

The flight test data were measured via a sophisticated miniature transducer/telemetry/recorder system which became temporarily available from another NASA test program. The transducers were of premium quality MilSpec grade and they were carefully calibrated by NASA Dryden Flight Research Center (DFRC) personnel. The transduced signals were sent via a subminiature 22-channel, pulse-code-modulated (PCM)/FM telemetry to a NASA-DFRC PCM recording van beside the test course. There it was converted to strip charts for on-line monitoring, input into an IRIG-standard 14-channel FM tape for data reduction at Systems Technology, Inc., and digitally stored for later NASA use. The time histories shown herein are from these later NASA-DFRC digital playbacks and include the detailed sensor calibrations.

Figure 2-3 identifies the various sensors and their locations in the Albatross II flight tests. Also shown are the temporary electric motor drive and its rechargeable NiCad batteries. With a few notable exceptions, the sensors recorded aircraft state variables without corrections for dynamics or location. The exceptions are:

- (1) The sonar altimeter (courtesy of Dr. Edwin Land of Polaroid Corporation) was installed near the aft bottom fuselage fin/fairing instead of the center of gravity (which is near the pilot's chest, just behind the tow-force sensor). Although it was accurate and reliable because of a logarithmically quantized output, it was of limited value for dynamic analysis.
- (2) The angle of attack and sideslip sensors were located about one chord above the wing chord plane, halfway along the nose boom, where the aerodynamic interference (from the canard downwash and wing upwash and sidewash) was felt to be minimal; however, this has not been computed. In addition, these sensors, and the true airspeed impeller, were subject to position effects from

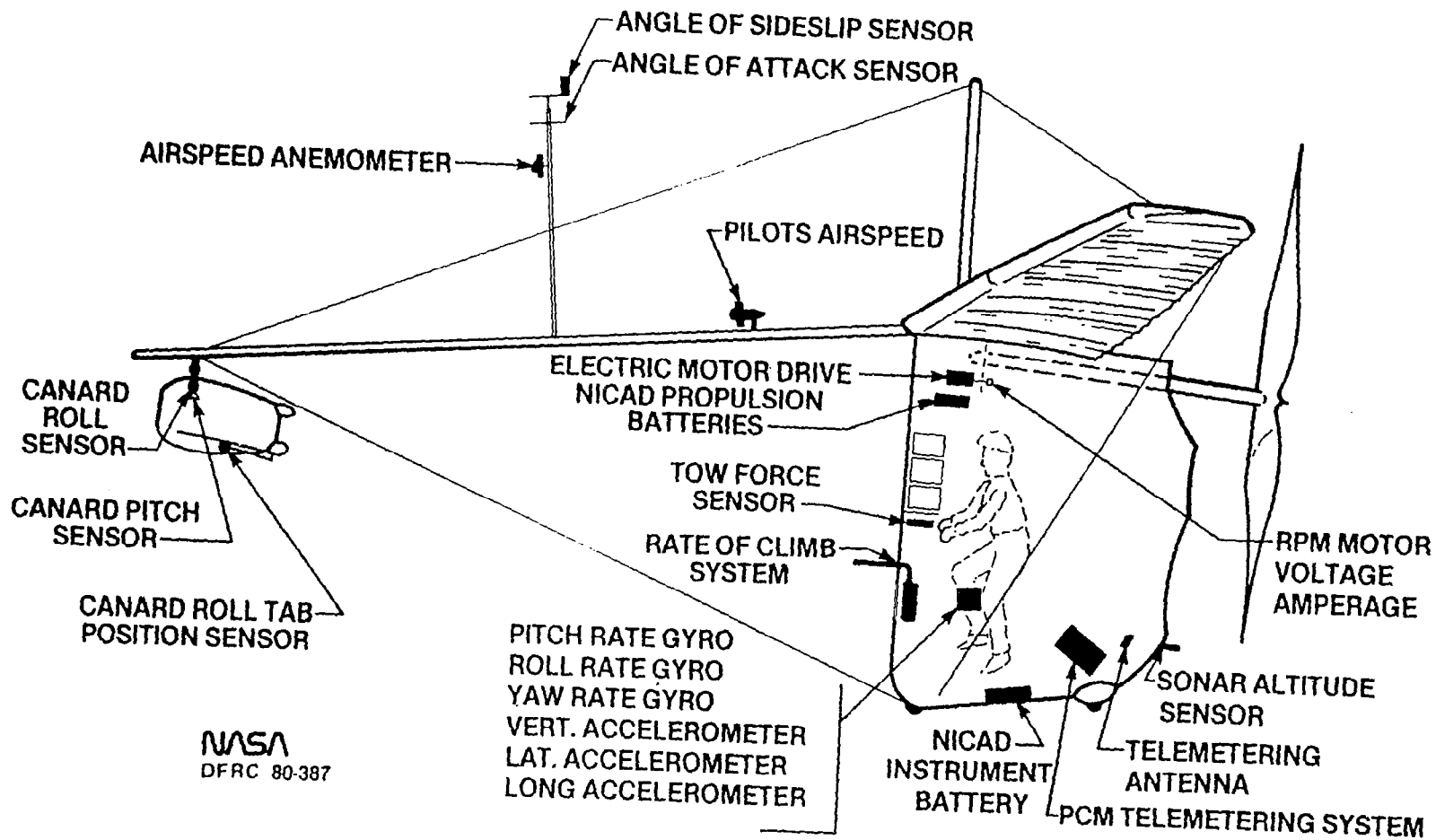


Figure 2-3. Gossamer Albatross Flight Test Instrumentation.

aircraft pitch, yaw, and roll rates. (The sensors were about 10 ft (3 m) above, and 23 ft (3.7 m) ahead of the effective center of gravity.) Although the α and β values clearly show that slight turbulence was encountered during the flight tests, these corrections were of sufficient complexity to preclude estimation of true α and β inputs in this limited scope program. The data are on Dryden Flight Research Center PCM archival files should someone be interested in such analyses at some future date. As shown in Section 3, pitch rate corrections to measured airspeed are very important above frequencies of 1/3 Hz.

- (3) The accelerometers were attached to the seat support near the main down tube and are sufficiently close to the center of gravity (about 1.5 ft below it) to not need corrections. However, they picked up excessive artifacts from the propeller-induced vibrations at 4 Hz. For this reason, the accelerometer data presented herein may have considerable errors.
- (4) The rate gyros were aligned parallel to the X, Y, and Z axes of the aircraft and were the primary motion response variables analyzed herein.

2.2 Procedures

All data flights were made early in the morning to avoid turbulence and thermal activity as much as possible. Because Rogers Dry Lake bed had been recently flooded, it was of insufficient strength to support the concentrated loads of the small wheels and of the operating crew's bicycles. It was thus necessary to perform the tests over the taxi strip near the NASA facility, where the thermal storage properties of the thick concrete produced some mild convective activity even on the calmest of mornings. In addition, the slight meteorological drainage flow towards the lake bottom past the hangars produced some large-scale (albeit slow speed) vortices which had an observed periodicity of about 20 to 40 seconds on different occasions. This residual turbulence significantly affected aircraft motions during both the performance and dynamic response runs, and rendered the former impractical to be analyzed within a small budget. Only a few portions of frequency-sweep data were obtained with sufficiently low turbulence to give reasonable results, and these are analyzed herein.

Each test flight followed the following plan:

- (1) Takeoff under battery power in about 10 to 20 feet (3 to 7 m) distance.
- (2) Climb to about 120 feet (3 m) ground clearance, as indicated by the sonar altimeter.
- (3) Execute a few test maneuvers, such as pitch elevator sweep, wing warp sweep, coordinated turns, over a predominately straight path and taking about two to three minutes.
- (4) Land, turn around and repeat the same cycle in the opposite direction.

The maneuvers performed by the pilot (Bryan Allen) were:

- o Frequency sweep (of elevator, wing warp, canard rudder tilt-tabs). Starting with about 16 seconds of a low frequency quasi-sinusoidal input wave, each succeeding wave or two was done at about one-half the period of the previous one (8, 4, 2, 1, 1/2 seconds). This gave a roughly logarithmic (one octave) progression of dominant frequencies, which is most efficient from the standpoint of frequency-domain system identification.
- o Coordinated turns. Using the combined anti-turn wing warp and pro-turn canard tilt, as described in the Appendix, a series of S-turns was made. Because the canard and warp deflections are closely proportional during such turns, the moments and forces from each are intrinsically confounded and such turns cannot be used to separate the warp and canard control derivatives. These data were used to verify the turn coordination scheme, but no detailed simulation of the actual flight cases was made.
- o Wing weight drops. In an attempt to test the apparent mass effects of the wing, a weight of 20 lb (9.1 kgw) was dropped from the mid-semispan

shortly after takeoff. Surprisingly enough, the additional weight did not seem to penalize performance very much, and the small roll, heave, and yaw accelerations it produced were nearly lost in the vibratory artifacts mentioned earlier.

- o Towed runs without propeller. Several runs were made with the propeller removed and a tow rope supplying the thrust required, this being measured by a tow force transducer in the aircraft near the CG (see Figure 2-3). The tow forces proved to be quite erratic, often varying as much as $\pm 50\%$ of the typical level. These variations were attributed to various causes, such as pilot control actions or gusts which affected the instantaneous drag level, apparent mass effects of gusts in the surge direction, and mismatch of tow-vehicle and aircraft airspeeds, especially under large-scale turbulence described earlier. It was also noticed on two towed runs during which canard control sweeps were made, that there appeared to be a reduction in the already neutral yaw stability, such that on one occasion a transiently divergent yaw-roll oscillation occurred. Such problems deterred the analysis of performance data from these tests.

A photograph of the Gossamer Albatross II in flight during a test is shown in Figure 2-4. Notice the following points: the early morning flight test period, flight speed compared to that of a bicycle, the trim attitude of the canard boom roughly parallel to ground, the momentary tilt of the canard rudder, the fairly caved and smooth airfoils and surfaces, and the location of the sensors for α , β , and airspeed atop the boom.

2.3 Data Reduction

The 22 channels of PCM telemetry were simultaneously recorded on digital tapes for NASA use, on two FM-IRIG 14-channel tape recorders for STI use (1-7/8 ips, 3.37 kHz center frequency), and on strip chart recorders for on-line use and annotation of pilot commentary.

The frequency response data given herein were reduced at Systems Technology, Inc. using its proprietary frequency domain analysis (FREDA) [Ref. 16]. Selected tape signals

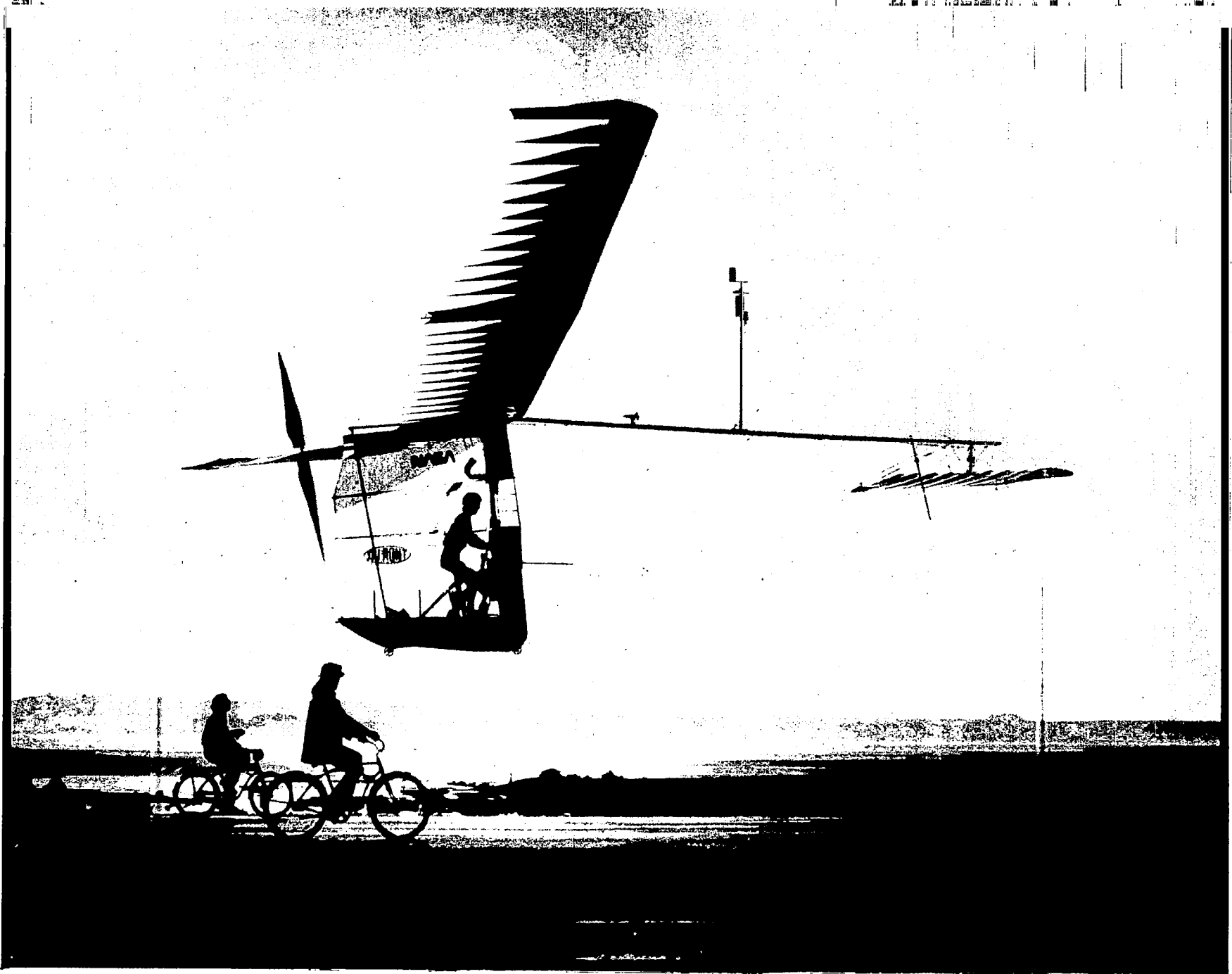


Figure 2-4. Gossamer Albatross-II in Flight During a Typical Test at NASA Dryden Flight Research Center.

were antialiased filtered at 40 Hz (first-order), digitized at various rates from 10 to 40 samples per second, and Fast-Fourier transformed to give 400 raw spectral frequencies. These were then grouped in "bins" of 3 to 5 Fourier frequencies per bin, and converted to power densities, transfer or describing functions (ratios of binned Fourier output/input vectors), and the coherency (linear dependence) of output and input signals. Experience shows that in such frequency sweep tests two conditions should apply for reliable frequency data points: high coherency between the input and output signals, and adequate power spectral density (not in the sensor noise). To facilitate evaluation of these, we have circled the best describing function points of high coherency and adequate power level in the data plots that follow. The other points may be of help in fairing the curves but cannot be trusted. We have also terminated the frequency response plots at frequencies beyond that where adequate input power existed.

3. RESULTS AND DISCUSSIONS

3.1 Longitudinal

3.1.1 Time History

Figure 3-1 is a reproduction of selected traces of the NASA-DFRC playback of the telemetered data from Flight 4 (19 March 1981), which tested the responses to a canard elevator frequency sweep. During the roughly 40 seconds analyzed (and noted on the elevator deflection trace), the control frequency was increased irregularly from about 1/8 Hz to 2 Hz (.8 to 12 rad/sec) with amplitudes from ± 2 to ± 7 degrees. The true airspeed fluctuated around 16 mph (23 ft/sec; 7.2 m/s). It is obvious from Figure 3-1 that the primary response variables such as pitch rate, normal acceleration, angle-of-attack, and rate-of-climb give strong and corresponding responses and, to a lesser degree, so do the airspeed and altitude.

The FREDA program for frequency responses, described in Section 2.3, was applied to this run with the results discussed below.

3.1.2 Pitch Rate Response

Figure 3-2 presents the standard format used on all frequency response data herein.

- At the top is the input's power spectrum, Φ_{ii} , each point or "bin" representing the average of the three to five adjacent Fourier frequencies. For Flight 4, the input spectrum*, $\Phi_{\delta_E \delta_E}$, is fairly broadband from about .8 to 12 rad/sec, in accord with the visual elevator trace noted earlier. Beyond 12 rad/sec, the frequency response data are considered unreliable, because the input signal is too low to provide an adequate signal-to-noise ratio. The "best quality" points herein are circled to emphasize them. The PSD is presented in Bode plot form, dB versus log-frequency, where 0 dB = 1 deg²/Hz.

*Capital identifier letters are used throughout this section to denote the measured variables, as distinct from the theoretical variables.

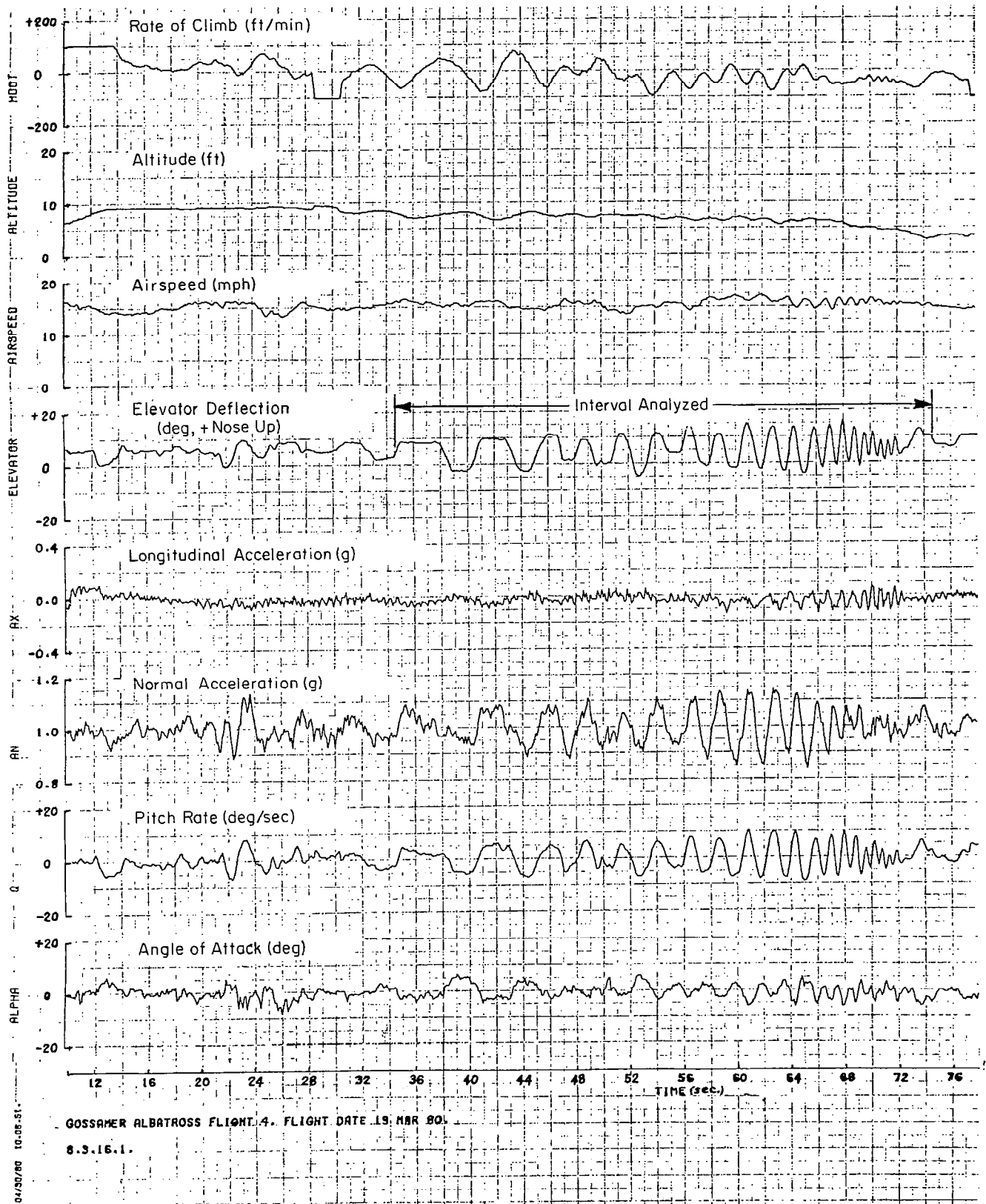


Figure 3-1. Time History of Flight 4 for Longitudinal Data.

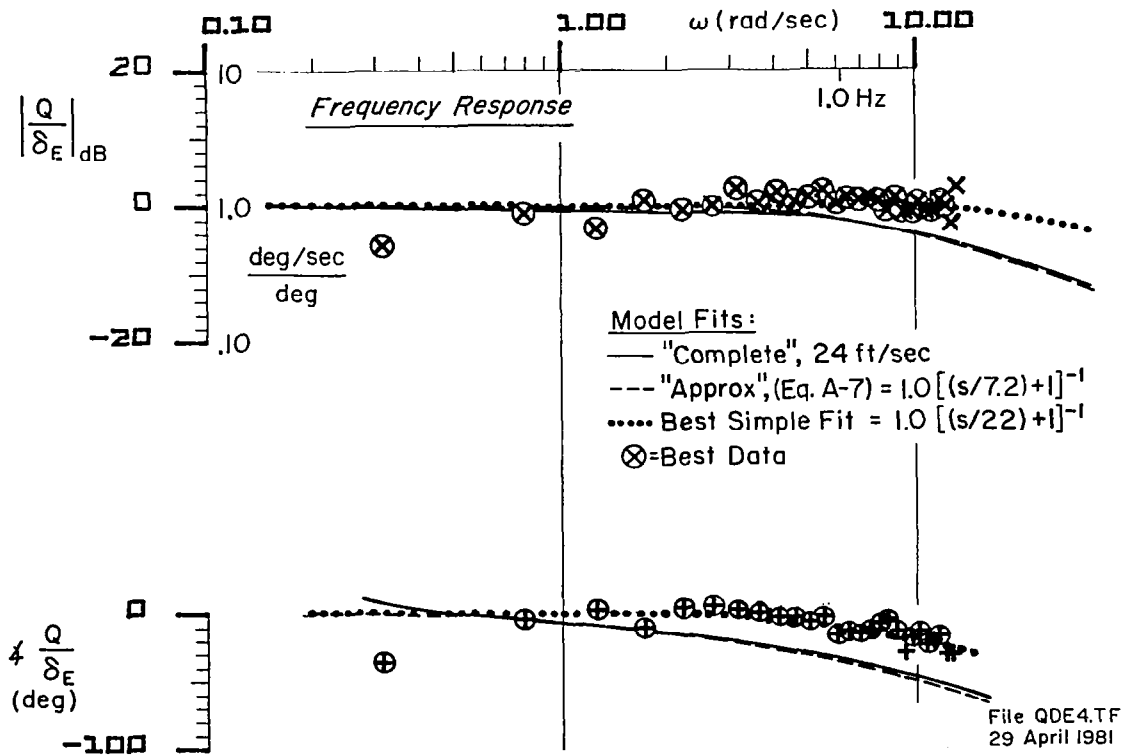
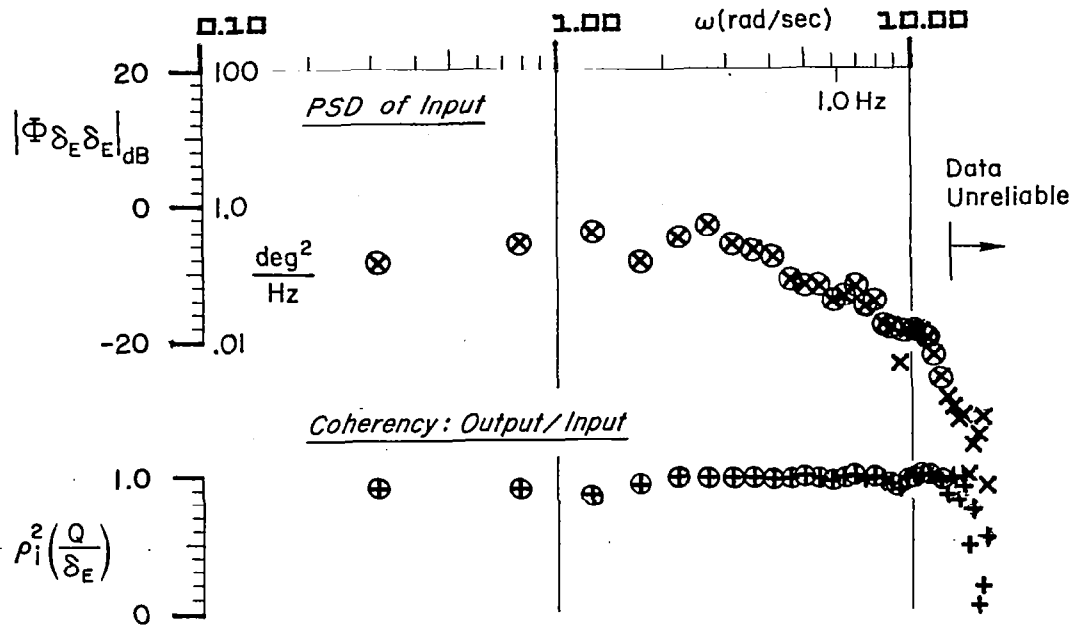


Figure 3-2. Pitch Rate Response to Canard Elevator Frequency Sweep.

- In the center is the coherency or fraction of the given output power (here, pitch rate) correlated linearly with the input across each frequency bin, $\rho_i^2 (Q/\delta_E)$. Generally, $\rho^2 > .80$ indicates input/output linearity, but the input PSD must also be adequate to provide reliable frequency responses. Here, the ρ^2 data from .8 to 12 rad/sec are generally $>.90$, indicating an excellent frequency sweep, with negligible response from causes other than the elevator deflection.
- At the bottom is the frequency response in Bode plot form (magnitude ratio in dB = 20 log magnitude, and phase in degrees, versus log frequency). Here, the pitch rate is almost precisely proportional to and in phase with the elevator deflection, as predicted by the theory in the Appendix.

Because no corrections are required to the measured pitch rate, these results can be compared directly with the computed predictions in the Appendix. On Figure 3-2 are shown three such model fits:

- a. "Complete" -- from the complete math model of the Appendix Section VI, B-2 interpolated for an airspeed of 24 ft/sec (closest to the flight speed).
- b. "Approximate" transfer function -- from Equations A-5 and A-7 for an airspeed of 20 ft/sec, whereby

$$\frac{Q}{\delta_E} \doteq \frac{U_o/l}{-\frac{s}{M_q} + 1} = \frac{1.0}{\frac{s}{7.2} + 1} \left[\frac{\text{deg/sec}}{\text{deg}} \right] \text{ at 24 ft/sec.}$$

- c. "Best" simple fit (by eye):

$$\frac{Q}{\delta_E} = \frac{1.0}{\frac{s}{22} + 1} \left[\frac{\text{deg/sec}}{\text{deg}} \right]$$

Both the complete and approximate models capture the essential trend of the data, but their phase lag is too large, while the amplitude of the complete model fits worse than the approximate case. Since there are negligible sensor dynamics, and the Appendix

shows the canard elevator is the dominant element, the cause must lie in the basic aerodynamics of the elevator. The theory assumes quasi-steady lift on the elevator, proportional to its net incidence (sum of deflection and pitch rate effects). Effects which might accentuate the short-term lift and produce less phase lag are "unsteady" lift effects due to the convection of bound vorticity downstream; build-up of tip-vortex-induced downwash; and apparent-mass effects due to the displacement of the semi-chord point relative to the pivot point [e.g., Ref. 6, following R.T. Jones]. These effects occur at mid-to-high frequencies, where the so-called oscillatory reduced-aerodynamic-frequency, $\Omega = (\omega c/2U_0)$, is on the order of 1.0. Here, $\Omega = 1.1$, so such unsteady lift effects may be significant. Another, possibly fortuitous, observation is that, if the aircraft-plus-pilot pitch inertia alone (163 slug ft²; Table A-2b) is used to compute M_q instead of the effective inertia (389 slug ft²), the approximate transfer function would have its mode at 17.2 rad/sec; much closer to the observed value of 22 rad/sec. Further analysis of the observed mismatch between the very reliable data and seemingly simple theory would seem to be warranted.

3.1.3 Normal Acceleration Response

Figure 3-3 presents the frequency response data for normal acceleration at the accelerometer location [about 0.4 ft (.15 m) ahead of the center of gravity] for Flight 4. Allowing for small differences in the sampling epoch, the elevator PSD at the top of Figure 3-3 is the same as in Figure 3-2, while the coherency $\rho^2(A_z/\delta_E)$ is worse, because the air gustiness and propeller vibrations contaminate the A_z signal. As before, the most reliable data are circled.

The circled frequency response points for A_z/δ_E reflect the computed transfer function for 24 ft/sec (7.3 m/s) as shown by the dashed line. (The A_z/δ_E transfer function is similar to, but not quite the same as, the \dot{h}/δ_e transfer function given in the Appendix, Table A-5). Although the match is not perfect, the general trends are correct, although the phase data show evidence of an additional delay effect.

Because no approximate transfer function analyses were made for A_z/δ_E , no discussion of the fitting errors is possible. However, we note that the mid-frequency fit (near $\omega = 5$ to 10 rad/sec) has some dependence in the break-frequency of $1/T_{sp1}$ which, in

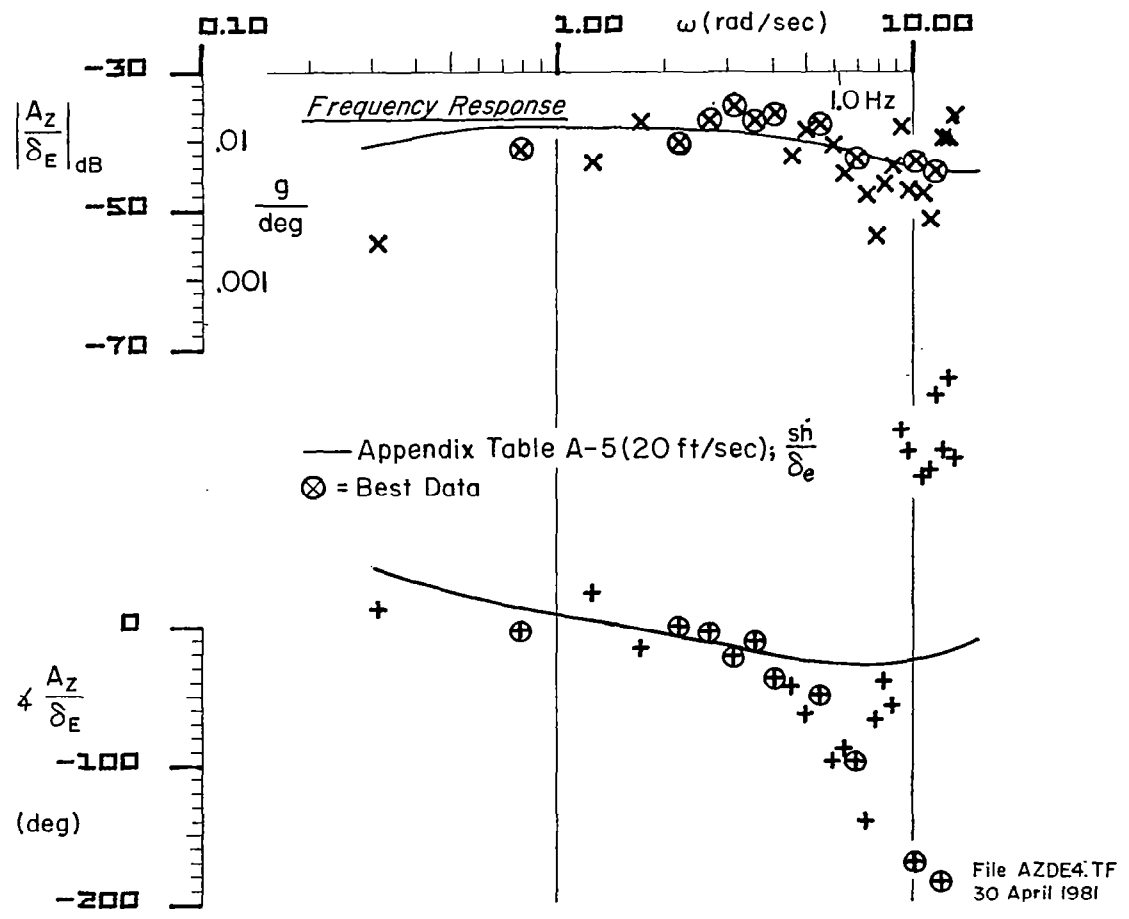
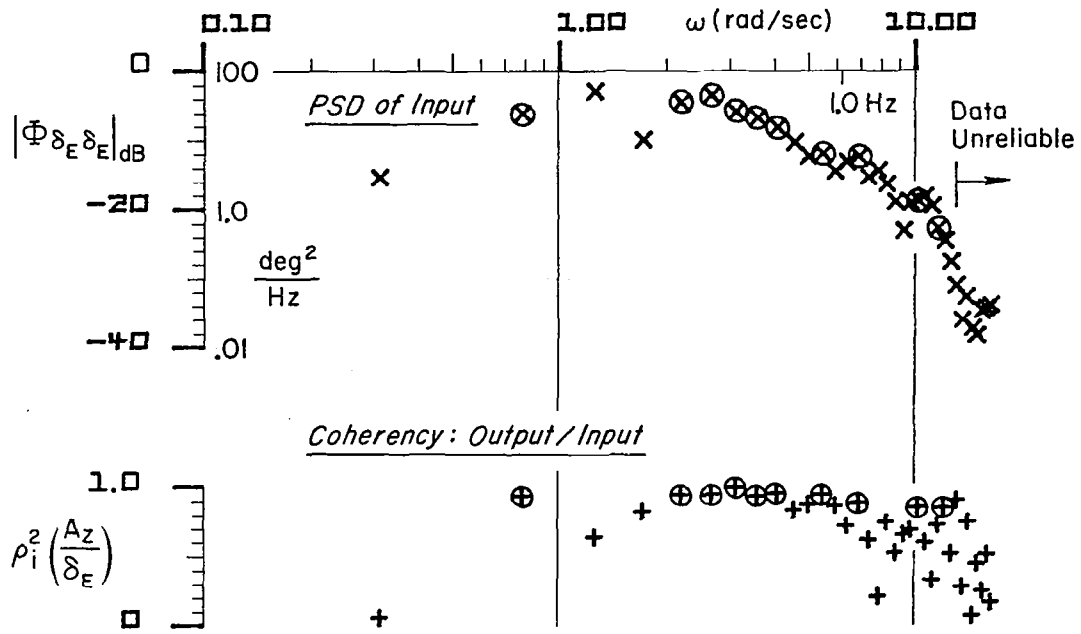


Figure 3-3. Normal Acceleration Response to Canard Elevator Frequency Sweep.

turn, is sensitive to the apparent mass term, Z_w^* . Further analysis of these effects should prove fruitful.

3.1.4 Airspeed Response

The airspeed sensor's response to the elevator sweep of Flight 4 is given in Figure 3-4, with best points circled, as before. While the elevator spectrum remains as before, the coherency, $\rho^2(U/\delta_E)$, is not as good, because the U signal was smaller and turbulence made it noisier. Because the airspeed transducer (a windmilling propeller) is located about 10 feet above the net center of gravity, it picks up a component due to pitch rate about the C_L [i.e., a positive airspeed increment for nose down (negative) pitch rate]. It can be shown that the airspeed response above 3 rad/sec is dominated by this component. In addition, the basic sensor has a response lag characterized by an approximately 2- to 3-foot (.6 to .9-m) spatial response distance lag. At 20 to 28 ft/sec (6.1 to 8.5 m/s), this amounts to an approximate sensor lag at .10 sec, or a break frequency at 10 rad/sec.

When these installation and sensor lag corrections were applied to the airspeed transfer functions, a drastic change from the Appendix values occurs. The resulting computed airspeed sensor responses are shown in Figure 3-4 for 20 and 24 ft/sec. Giving some credit to the low-frequency points, it can be seen that the essential nature of the airspeed response to elevator can be adequately caught by the theory with proper corrections for sensor locations and response lag.

3.2 Lateral-Directional Data

3.2.1 Responses to Wing Warping

3.2.1.1 Time Traces

The only usable data for wing warping responses were obtained from Flight 15, whose time history is given in Figure 3-5 (latter portion). There were inadvertent canard rudder tilt inputs along with the desired warp inputs, and this may have "distorted" the response to warps over the full 32-second analysis period. Consequently, a shorter (13-second) portion was analyzed wherein the canard deflections were less correlated with the warp inputs.

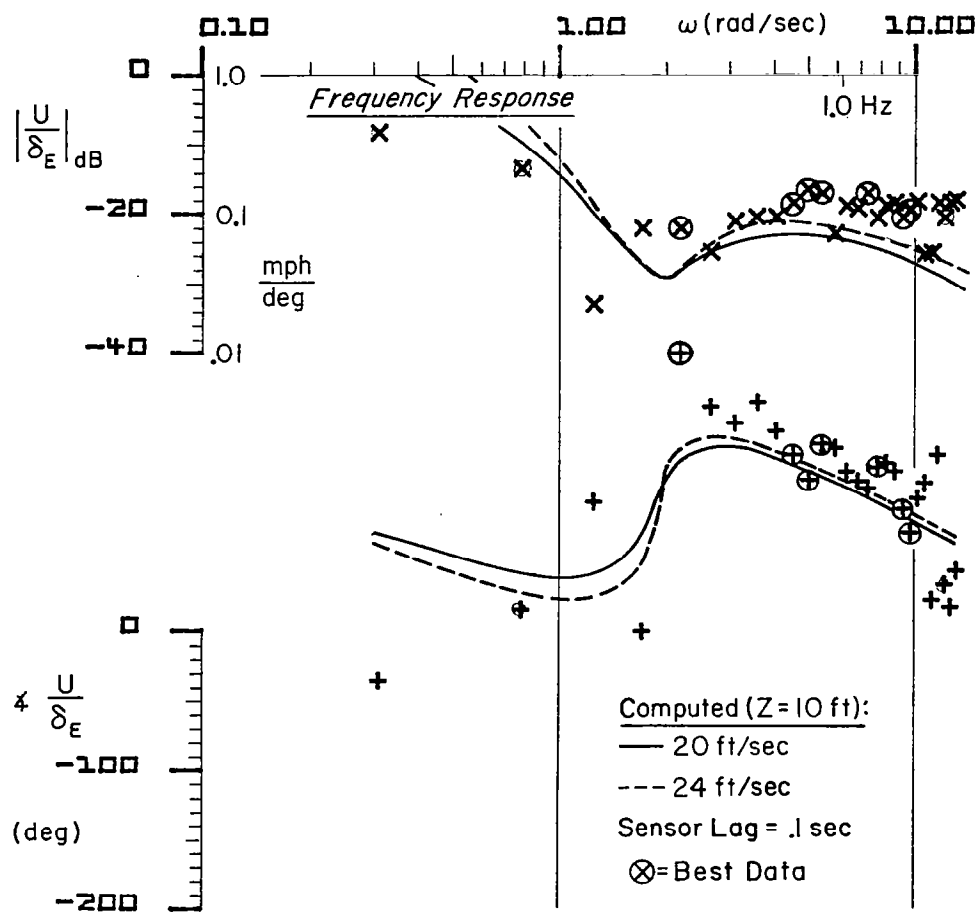
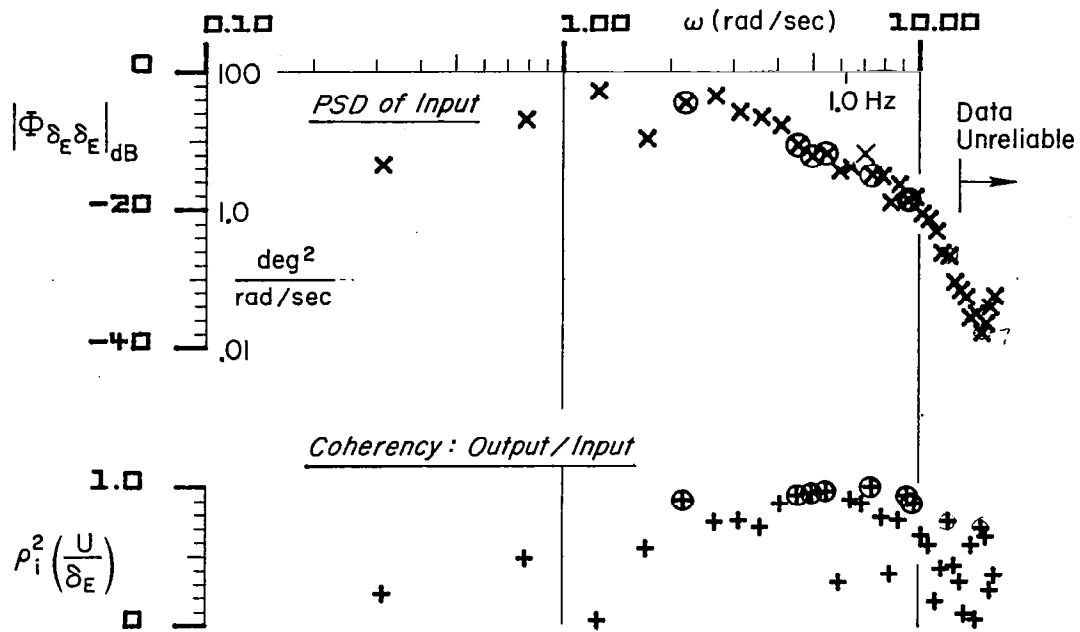


Figure 3-4. Sensed Airspeed Response to Canard Elevator Frequency Sweep.

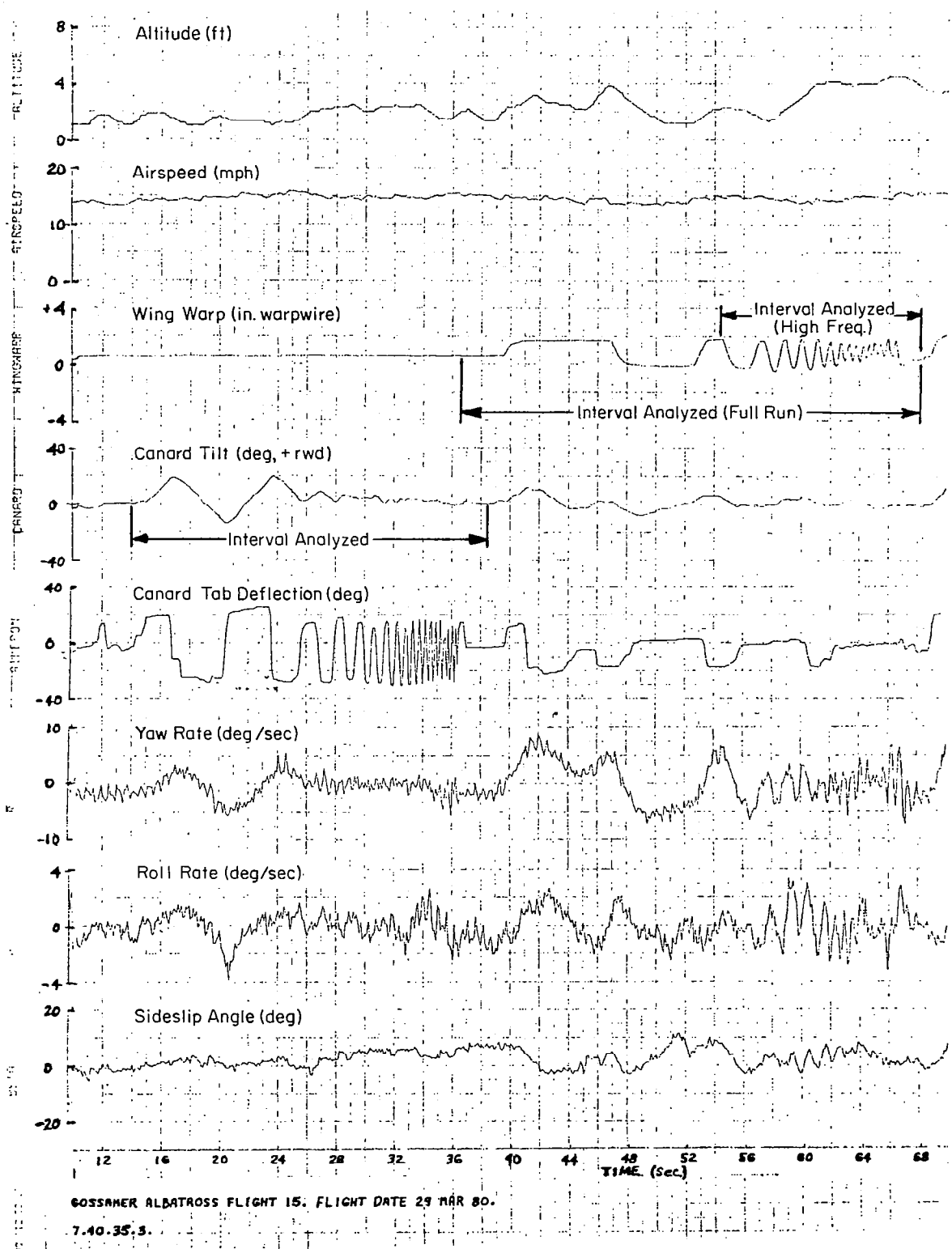


Figure 3-5. Time History of Flight 15 for Lateral-Directional Data.

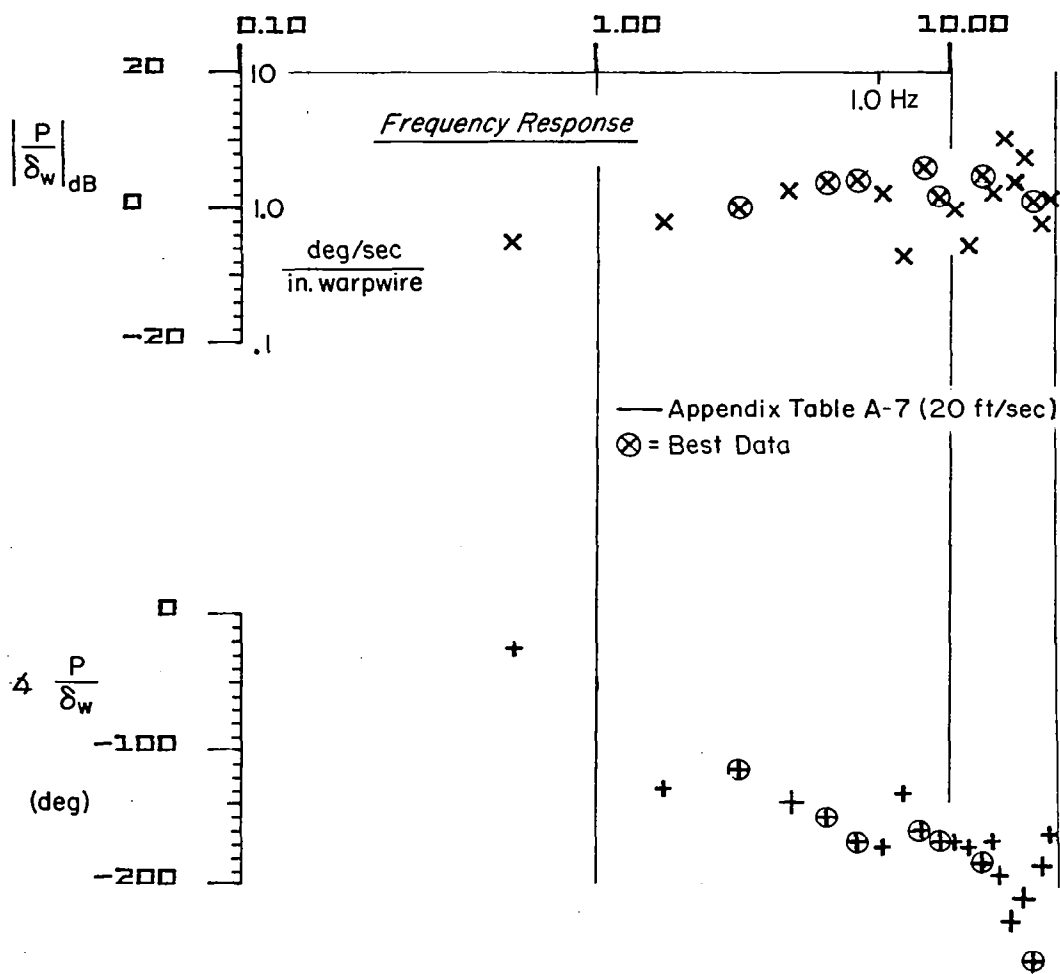
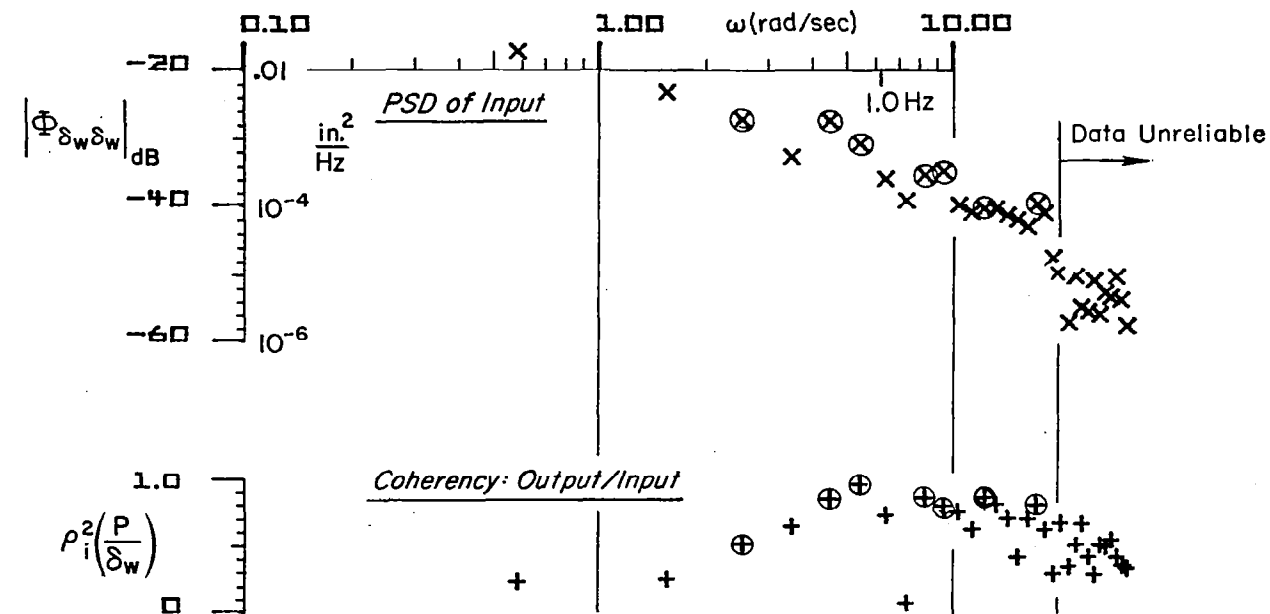
It was noted, by the pilot (Bryan Allen) and the principal author observing this flight, that at the higher wing warp frequencies (near 2 to 3 Hz) an aeroelastic mode of the wing may have been excited, but the effects of this on the data are not known.

The effective geometric warp, induced by differential warp wire travel, could not be precisely measured because it is affected by lift loads not duplicatable during surface calibrations. The estimated values lie in the range of ± 2 to 4 degrees per wing (or 4 to 8 degrees total differential warp) for one inch (2.54 cm) of warp wire deflection, depending on the assumed wing flexibility.

3.2.1.2 Roll Rate Response to Wing Warp

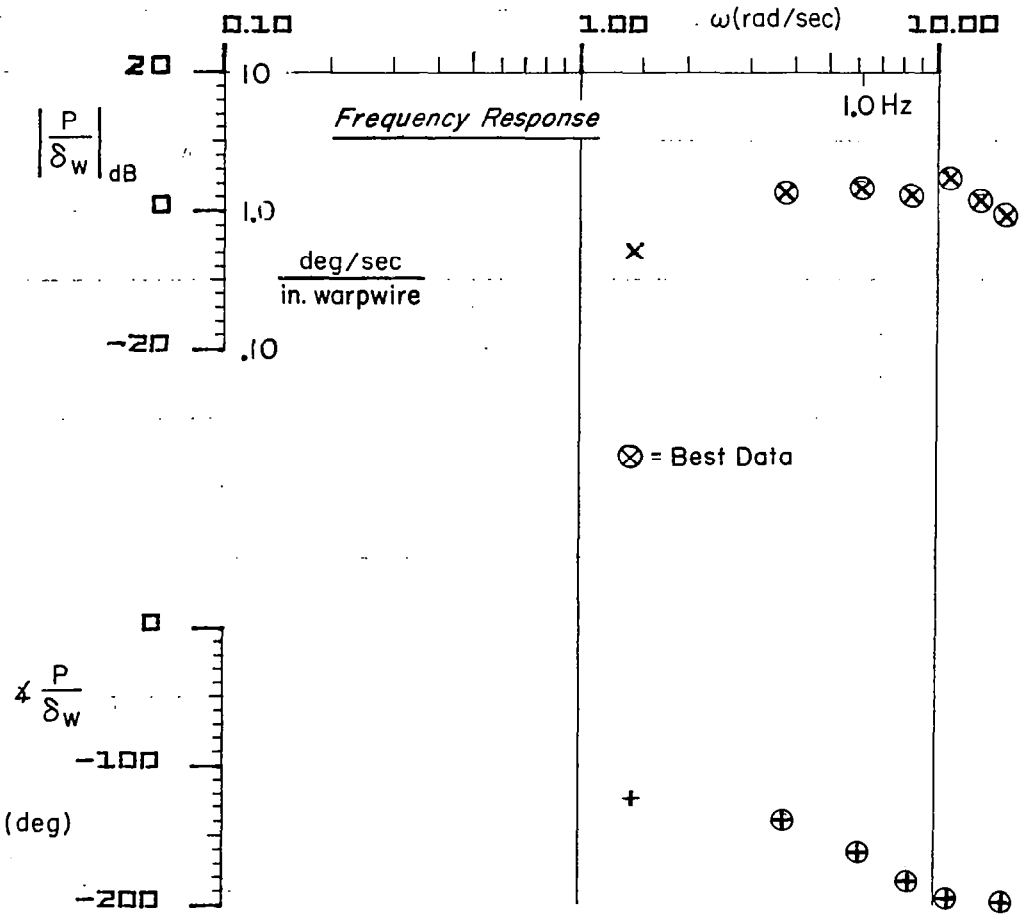
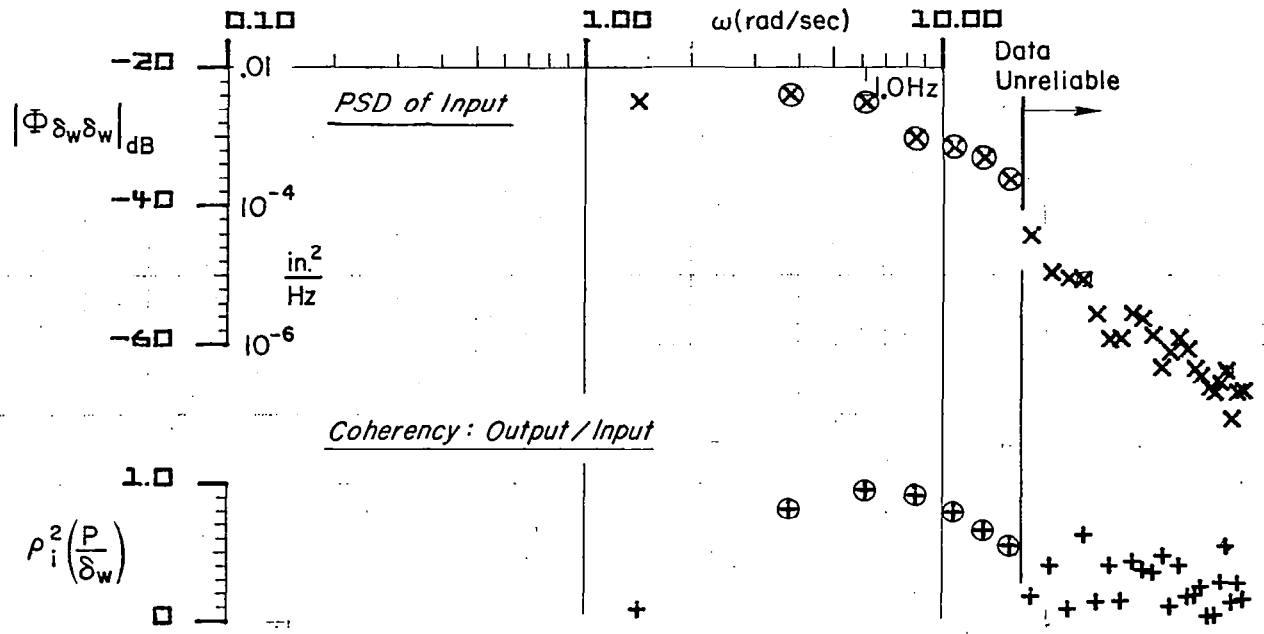
The reduced roll rate response data are shown in Figures 3-6 and 3-7, the latter for the last 13 seconds, as noted above. For the longer period (Figure 3-6), the PSD of the warp input sweep indicates high power at low frequencies, but the coherency is poor, thereby discrediting the lowest pair of frequency points. The most trustworthy points are circled as in earlier plots. The corresponding data from the last 13 seconds (higher frequency portion of the sweep) are given in Figure 3-7. The collected set of reliable points from both analyses is summarized in Figure 3-8.

The combined data show fairly good agreement, considering the modest coherency of many points, especially the low frequency ones. While the "ideal" roll rate response to warp (wing rolling at the twist helix angle) is about 3 to 4 deg/sec per inch of warp wire control, with roll rate in phase with δ_w , the measured values are highly reduced and distorted due to the warp hysteresis, low directional stability, and the complex roll/yaw dynamics discussed in the Appendix. Comparisons of the data of Figure 3-8 with the computed transfer function from Appendix Table A-7, indicates that the correct magnitudes exist but there are significant differences which have not yet been explained. The departure of the amplitude and phase data from the computed curve above 1 Hz is consistent with a structural model excitation at about 2 Hz, but this has not been analyzed.



File PDW15, TF2
 8 May 1981

Figure 3-6. Roll Rate Response to Wing Warp Frequency Sweep (whole 32 sec; Flight 15).



File PDW15.TF
1 May 1981

Figure 3-7. Roll Rate Response to Wing Warp Frequency Sweep (last 13 sec of Flight 15).

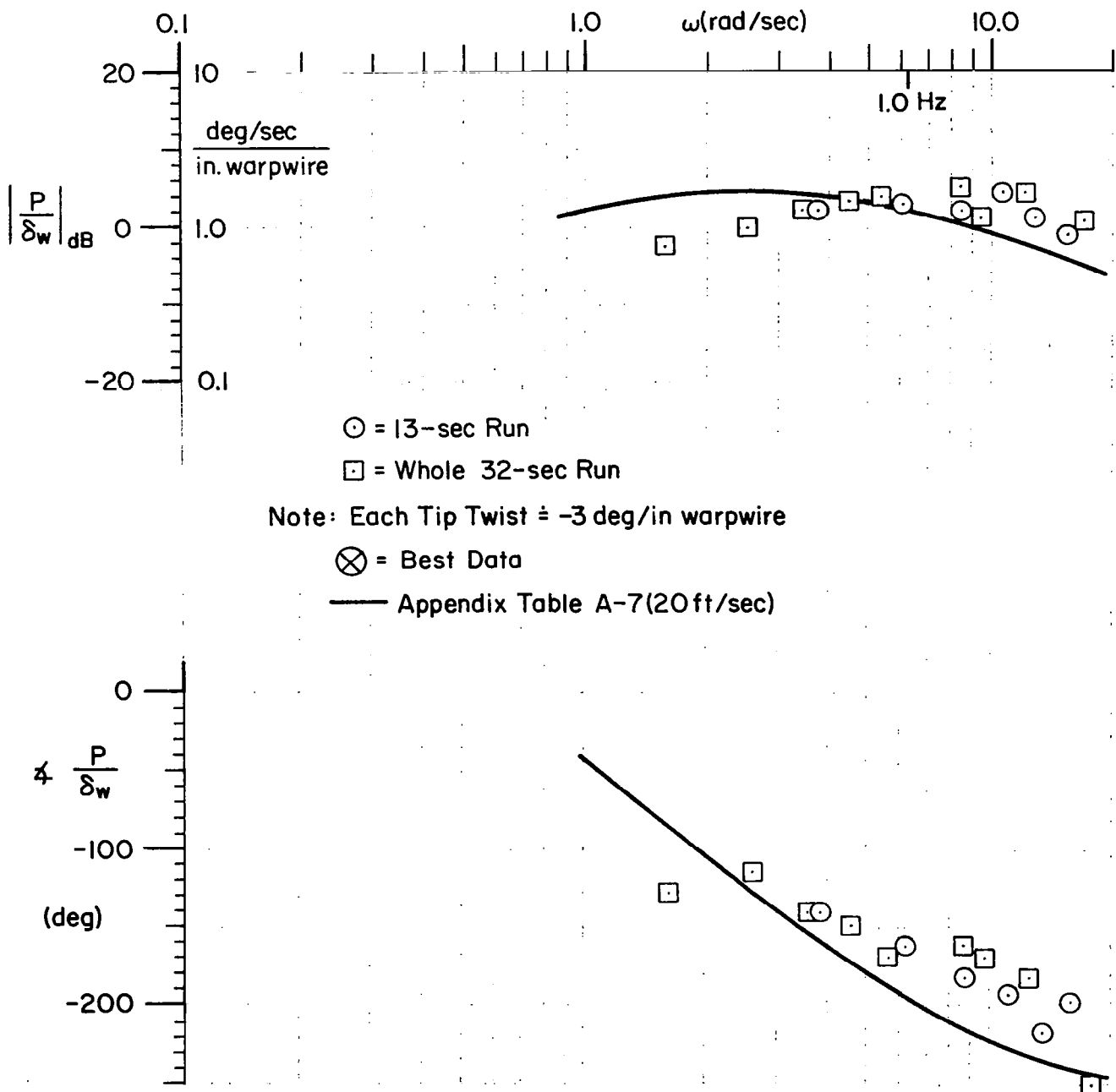


Figure 3-8. Summary of Best Data for Roll Rate Response to Wing Warp.

3.2.1.3 Yaw Rate Response to Wing Warp

The frequency response data for yaw rate from wing warp is given in Figure 3-9. These data suggest a yaw rate roughly proportional to warp across the .2 to 2 Hz frequency band, with a possible underdamped break near 1.5 Hz (10 rad/sec). Thus, contrary to conventional aircraft, the wing warp control provides wideband yaw rate control, as discussed in the Appendix.

The detailed frequency response does not match well with the transfer function inferred from Appendix Table A-7. The gain is low, probably because the adverse yaw effects were overestimated. As in the roll response, there is evidence of an elastic mode excitation at about 15 rad/sec, resulting in a high gain and phase "dip" there.

3.2.2 Responses to Canard Rudder Tilting

Data from two flights were used for the responses to canard rudder tilt. The early portion of Run 15, shown already in Figure 3-5, provided a fairly wideband tilt input from roughly .1 to over 2 Hz, while Flight 6, shown in Figure 3-10, has better low frequency data. Both sets were contaminated by appreciable air turbulence, as indicated by the fluctuations in the sideslip-sensor traces on Figures 3-5 and 3-10.

The canard wing is pivoted freely in roll and is tilted by pilot control of two canard aileron tabs. The canard response to tab deflection is like that of a very light wing surface, with ailerons, such that the canard's roll rate is closely proportional to tab deflection with an effective roll time-constant of about 0.1 sec:

$$\frac{\dot{\phi}_R}{\delta_{\text{tab}}} = \frac{\dot{\delta}_R}{\delta_{\text{tab}}} = \frac{.44}{.1 \text{ s} + 1} \left[\frac{\text{deg/sec}}{\text{deg}} \right].$$

The canard tilt rate, $\dot{\delta}_R$, relative to the vehicle, is closely approximated by the absolute canard roll rate, $\dot{\phi}_R$, because the vehicle roll rate is negligible by comparison.

Because the transfer functions in the Appendix are given as a function of canard tilt angle and because the canard aileron tab data recorded were on a separate tape from the

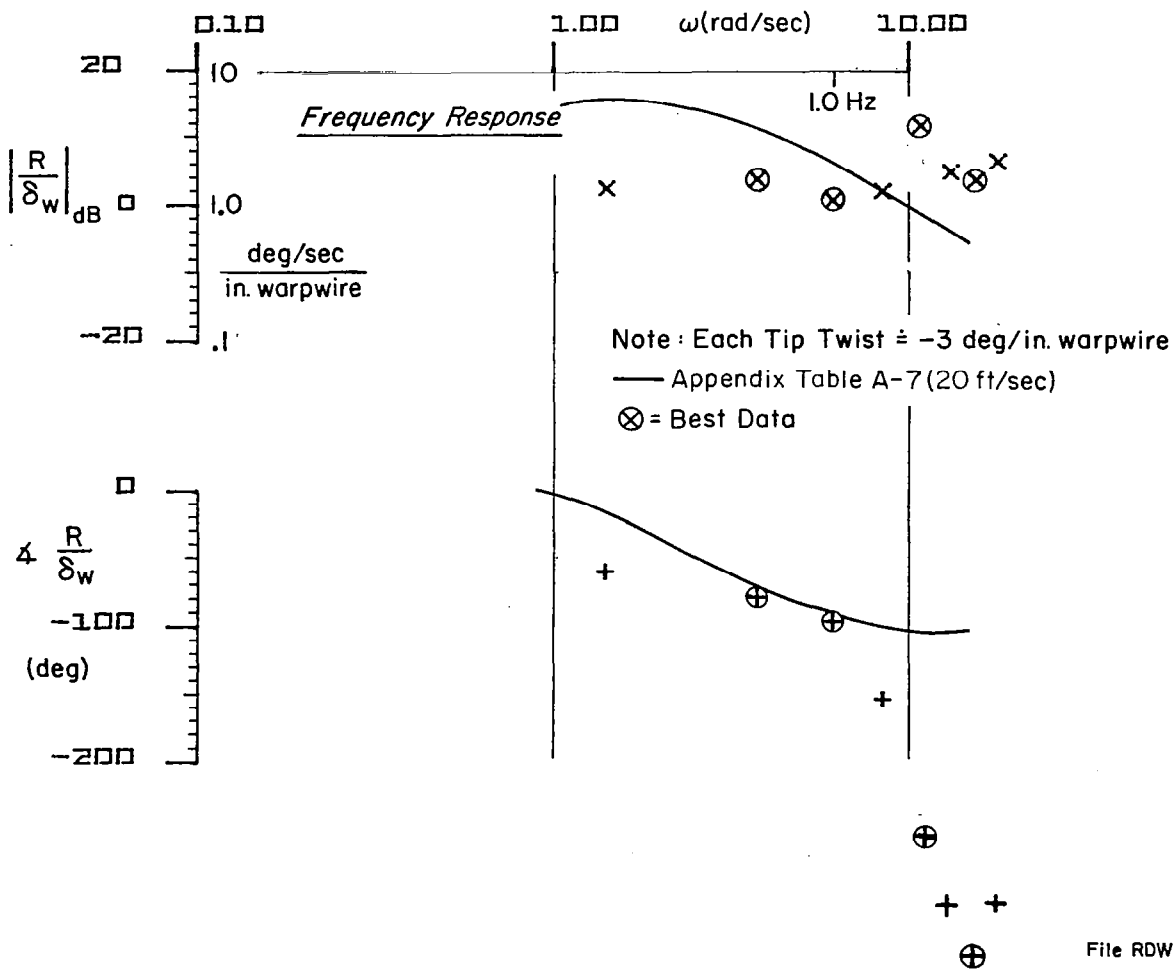
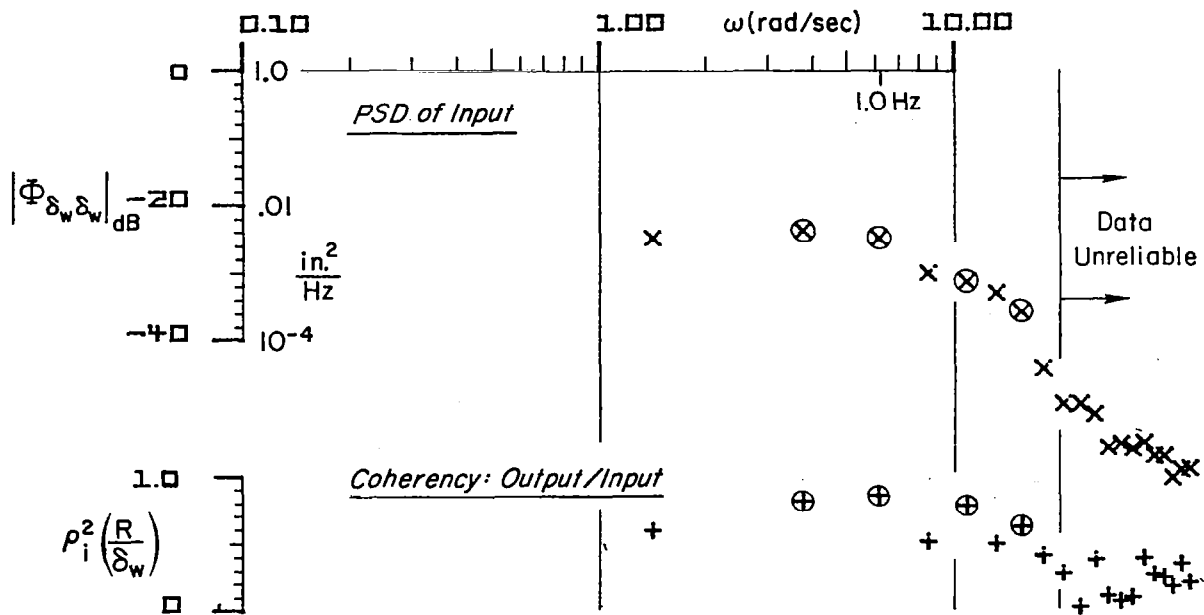


Figure 3-9. Yaw Rate Response to Wing Warp (last 13 sec of Flight 15).

File RDW15.TF

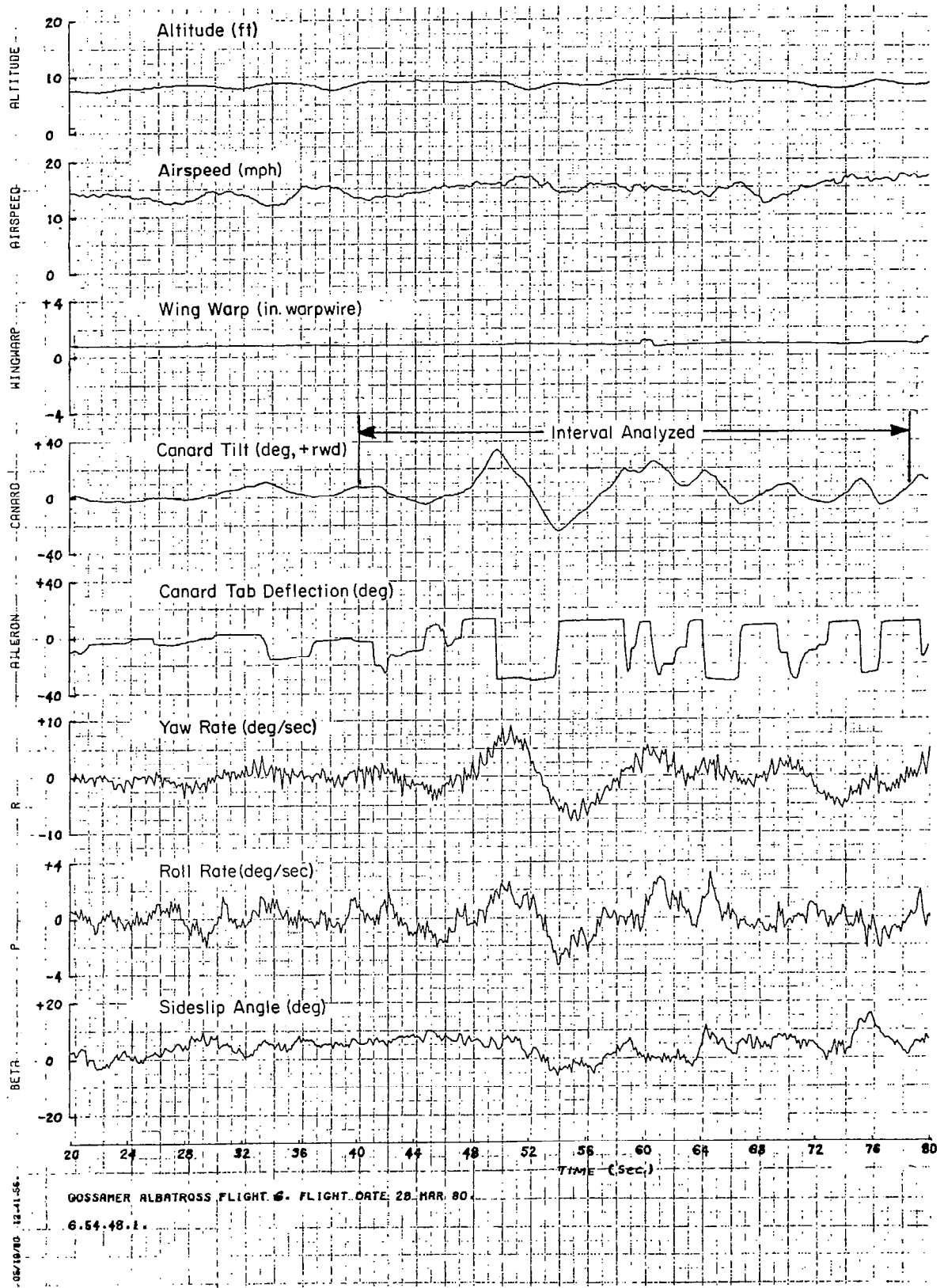


Figure 3-10. Time History of Flight 6 for Canard Tilt Data.

main data, the frequency responses were computed with respect to the measured canard tilt angle.

3.2.3 Yaw Rate Response to Canard Tilt

Figure 3-11 shows the lower frequency data from Flight 6. Even though the time history clearly shows strong aileron tab inputs to 3 Hz (20 rad/sec), at higher frequencies the canard's tilt response is attenuated across frequency, so that the measured tilt angles reduce to the noise level; thus, Flight 15 data are unreliable beyond about 1 Hz. The higher frequency data from Flight 15 are given in Figure 3-12. Here, there is a distinct peak in coherency and control spectra near 3 Hz (20 rad/sec), so a typical frequency response point has been included.

The summary of reliable yaw rate response data is given in Figure 3-13, where it is seen that both flights give overlapping results. As mentioned in the Appendix, the vehicle's basic yaw rate response must fall off at higher canard tilt frequencies due to inertial effects, but the present data does not show that, at least in the magnitude plots. The apparent anomaly may be due to damped structural deformation modes excited by canard side forces (e.g., due to boom bending or twisting). The theoretical yaw rate response from the Appendix Table A-7 is shown in Figure 3-13 for the 20 ft/sec case.

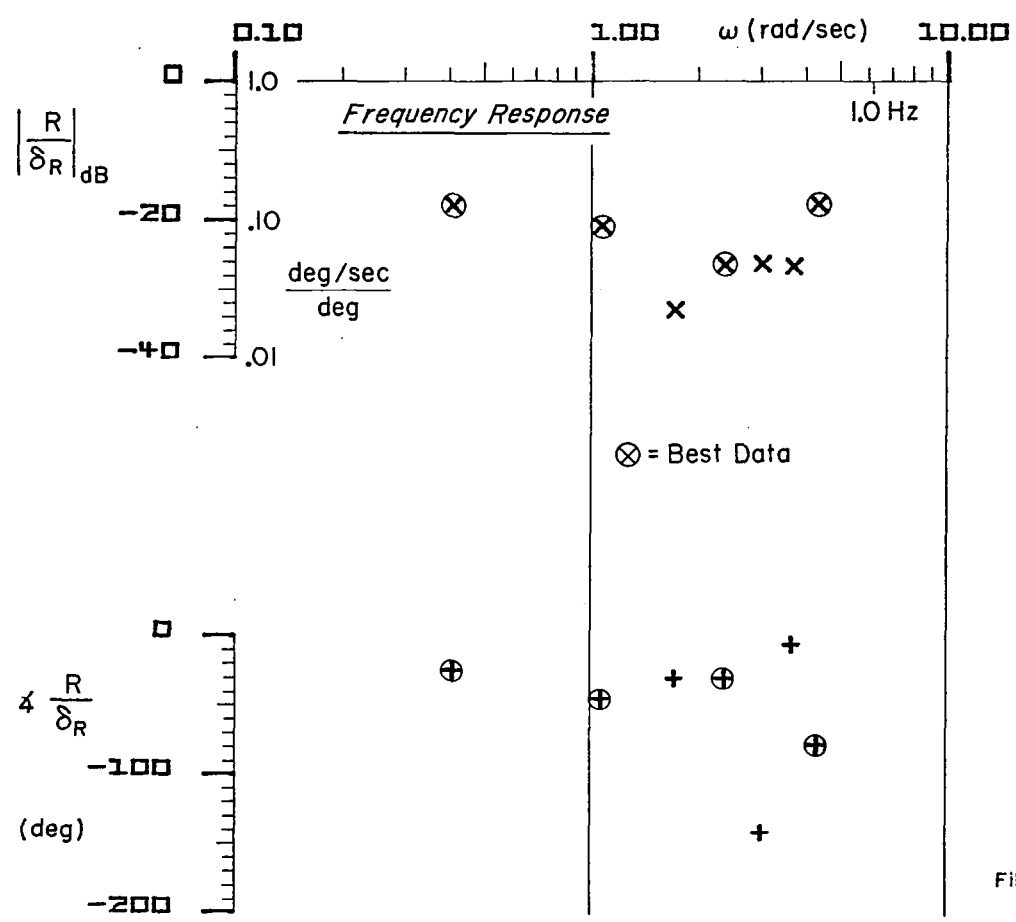
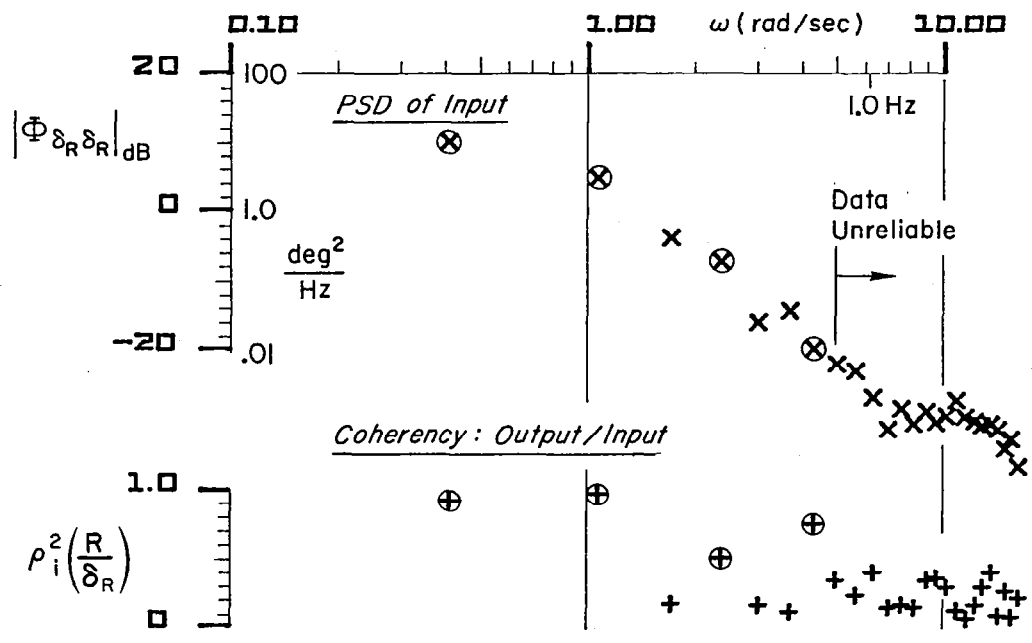
From these tests, the yaw response to canard tilt can be modeled most simply by a constant gain of about 0.10 deg/sec of yaw rate per degree of tilt, in series with a pure (transport) delay of about 0.3 sec:

$$\frac{R}{\delta_R} \doteq .10 e^{-.3s} \left[\frac{\text{deg/sec}}{\text{deg}} \right] .$$

This approximation is shown dotted in Figure 3-13, from which it is apparent that it fits the magnitude data up to about 1 Hz and the phase up to 3 Hz.

3.2.4 Roll Rate Response to Canard Tilt

The roll rate induced by the yawing motions from tilting the canard is the primary means for controlling the Gossamer Albatross in roll. The frequency response data for



File RDR6.TF2

Figure 3-11. Yaw Rate Response to Canard Tilt Frequency Sweep; Flight 6.

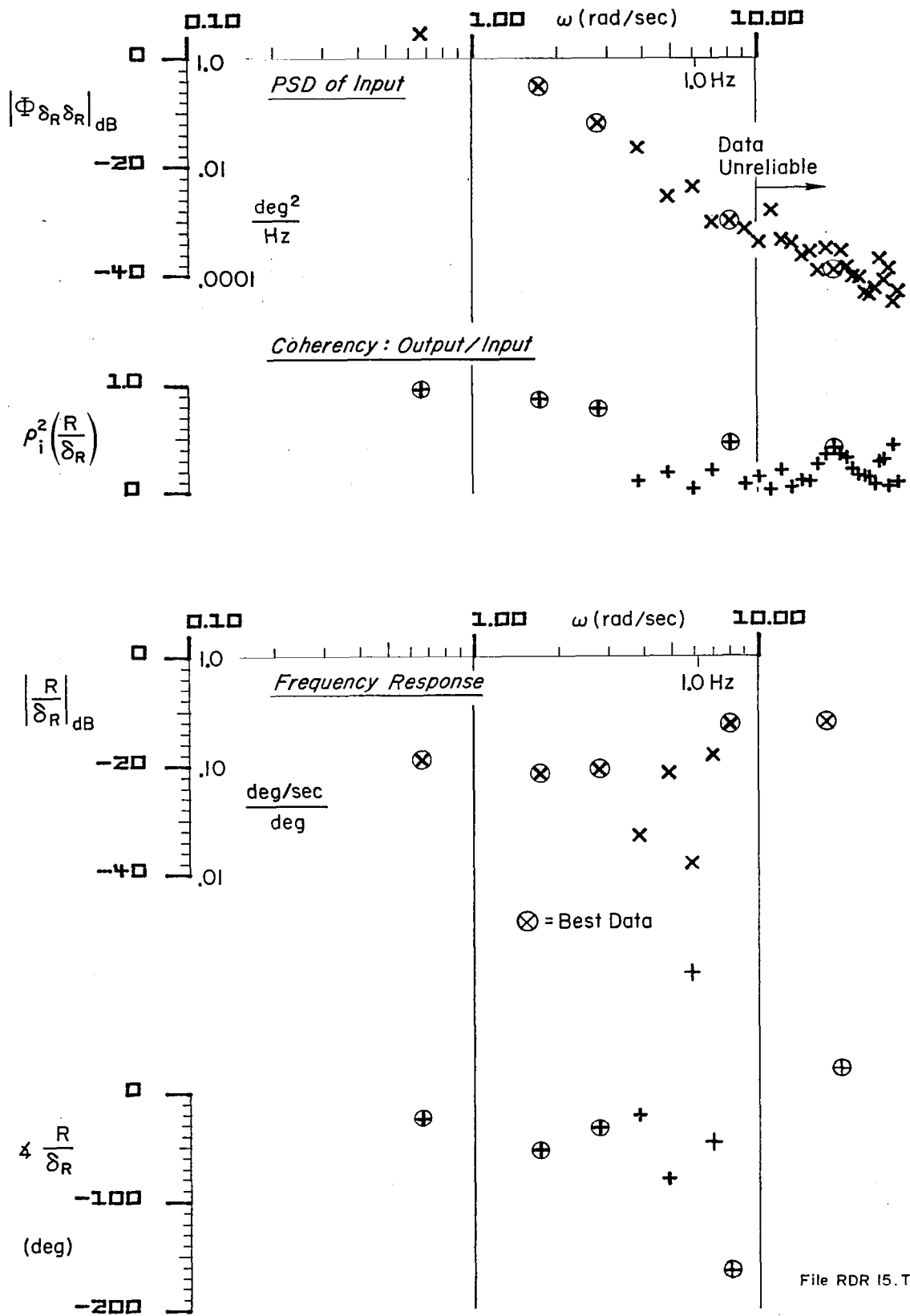


Figure 3-12. Yaw Rate Response to Canard Tilt Frequency Sweep (last 13 sec of Flight 15).

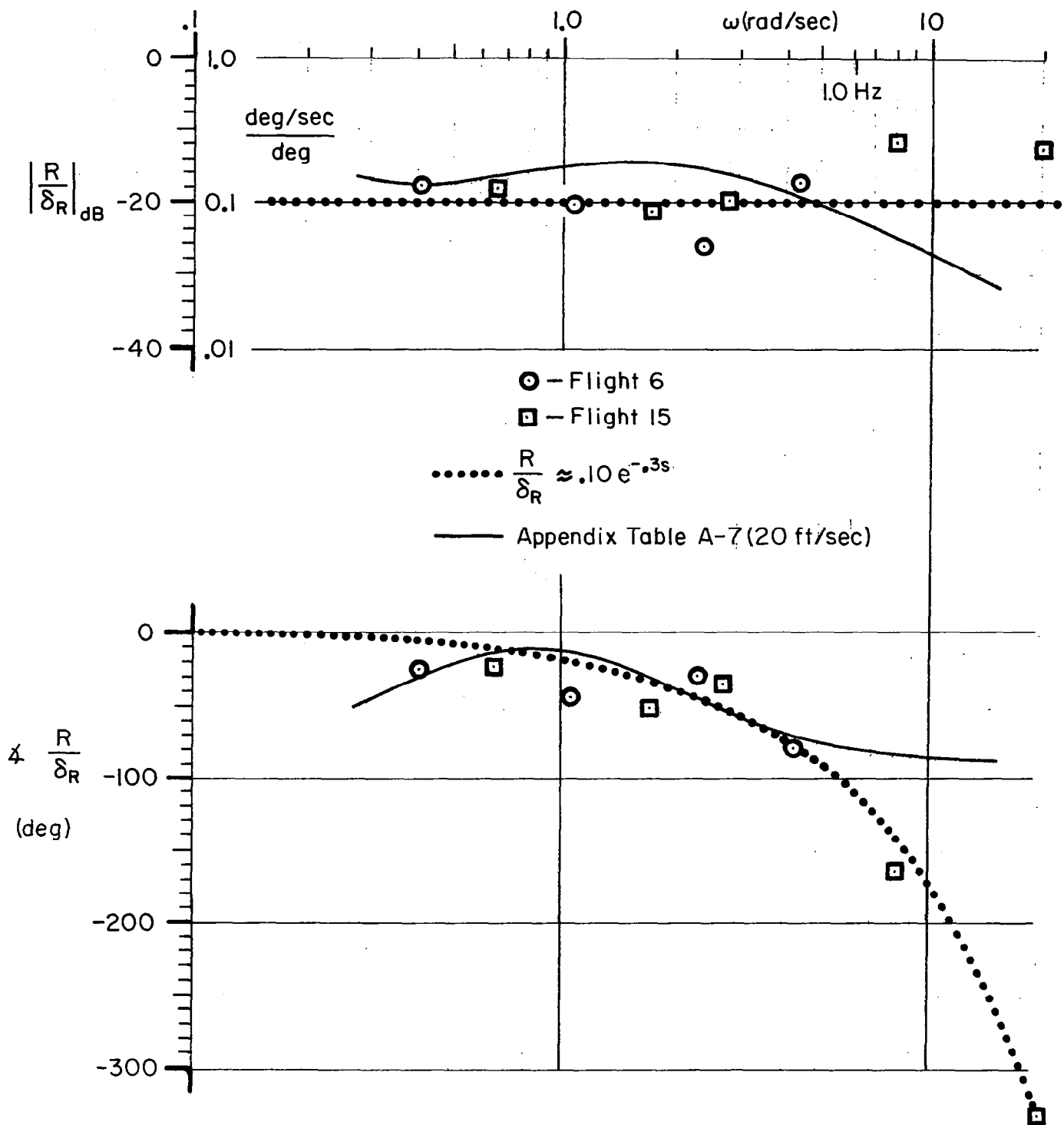


Figure 3-13. Summary of Best Data for Yaw Rate Response to Canard Tilt.

Flights 6 and 15 are given in Figures 3-14 and 3-15. The control input PSDs differ slightly from those in Figures 3-11 and 3-12 because of slightly different analysis starting times; and the coherencies are lower, especially at higher frequencies. Consequently, only seven truly reliable points are identified in the summary plot of Figure 3-16, but these agree fairly well between the two flights.

An interesting observation was made in comparing the yaw and roll responses from each flight: most of the frequency response points below about 2 Hz (10 rad/sec) are quite similar; even the less coherent points. This occurs because the roll rate is caused primarily by the yaw rate through the rolling-moment-due-to-yawing coefficient, C_{ℓ_r} , as discussed in the Appendix. The foregoing being true, the similar fit of the same approximate transfer function used for yaw rate response is not surprising, but the fact that the same gain matches both is coincidental. Also shown are the 20 ft/sec computed transfer function from Appendix Table A-7 for 20 ft/sec:

$$\frac{P}{\delta_R} \doteq .10 e^{-.35 \left[\frac{\text{deg/sec}}{\text{deg}} \right]} .$$

The general prediction of roll rate proportional to tilt angle up to about 1/2 Hz (3 rad/sec) is seen to be true, but the measured gain is about 35% (3 dB) higher than predicted. As in the yaw rate response at higher frequencies, the phase seems to be as predicted, while the amplitude is higher, perhaps due to elastic overshoot effects. Larger tilt inputs at frequencies above 6 rad/sec (1 Hz) would be needed to resolve these issues, but they are hard to get and not of great importance for the control of these vehicles at low speeds.

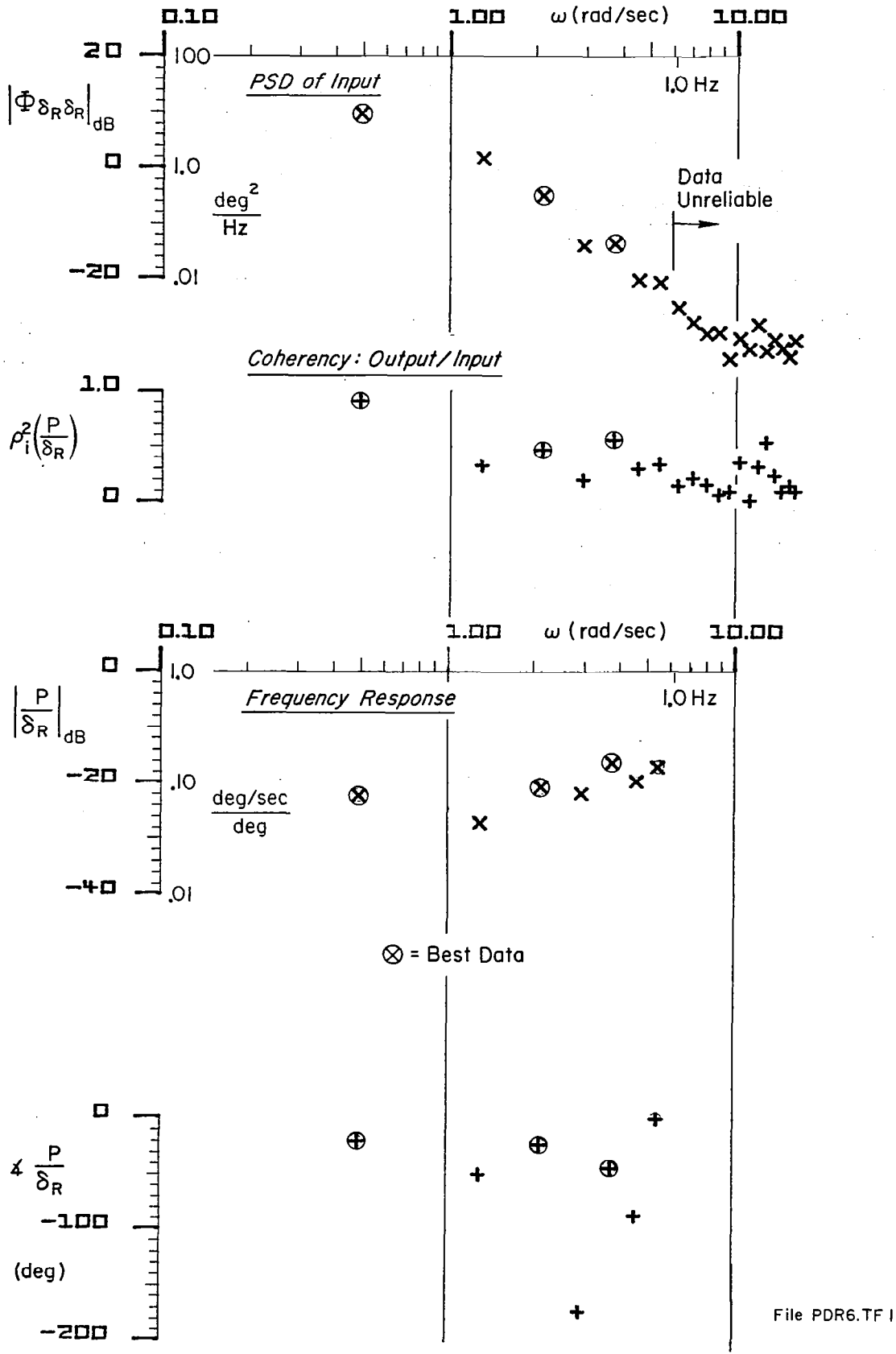


Figure 3-14. Roll Rate Response to Canard Tilt Frequency Sweep; Flight 6.

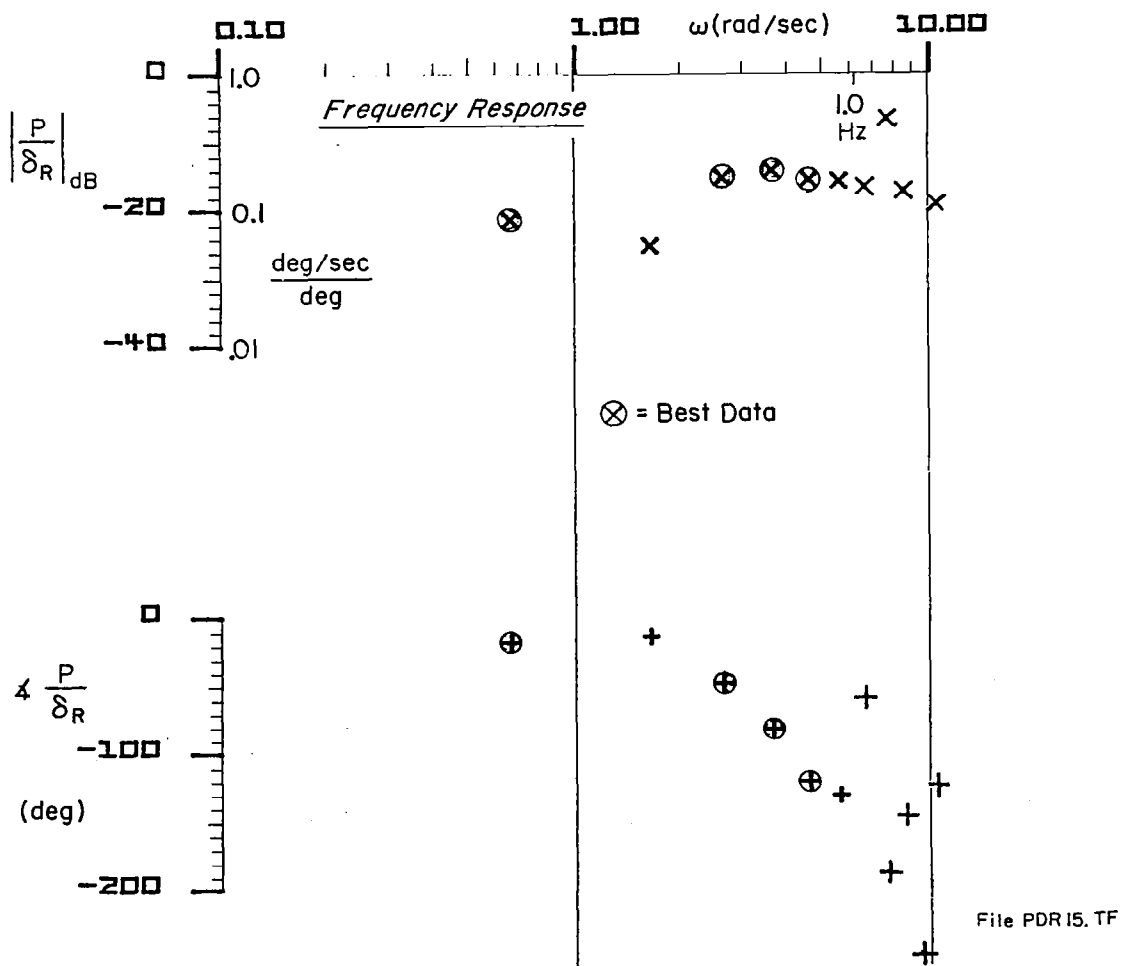
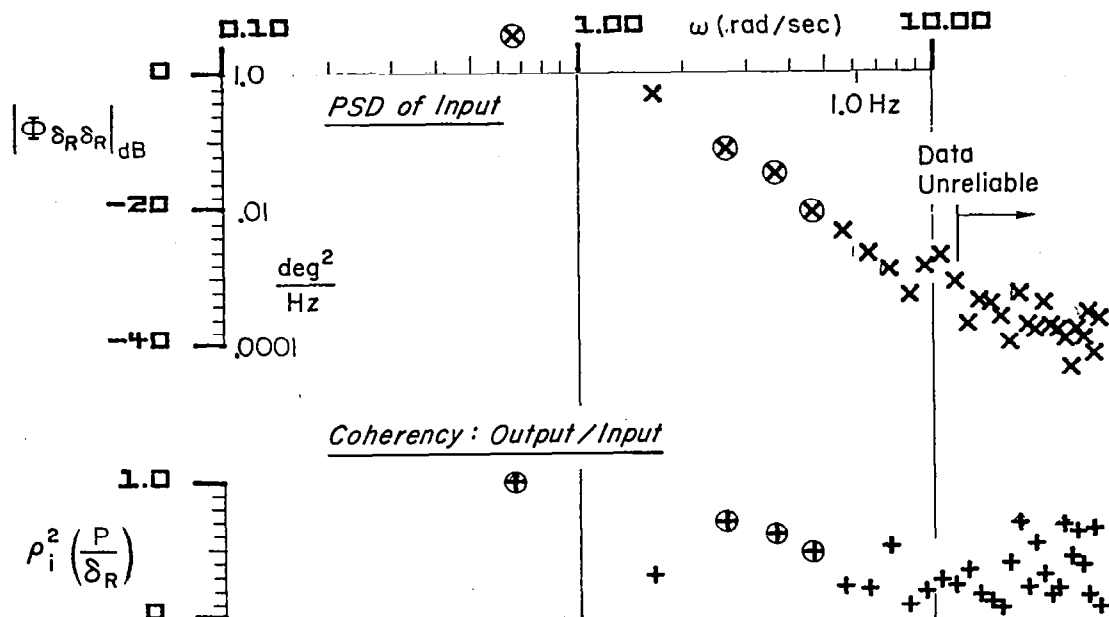


Figure 3-15. Roll Rate Response to Canard Tilt (last 13 sec of Flight 15).

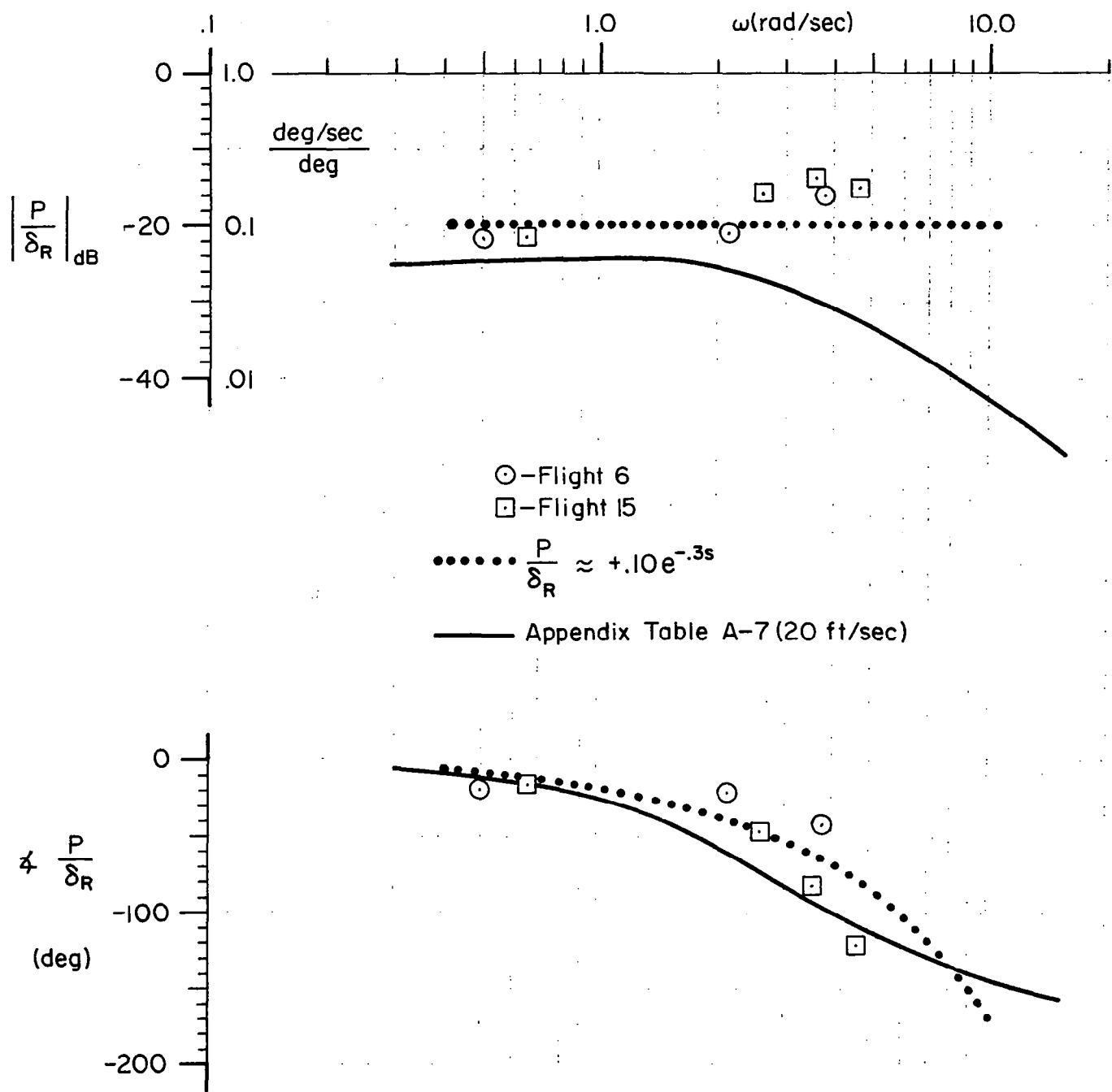


Figure 3-16. Summary of Best Data for Roll Rate Response to Canard Tilt.

4. CONCLUSIONS AND RECOMMENDATIONS

A series of brief analyses and flight tests has been made to reveal the dynamic response to controls of the Gossamer Condor and Gossamer Albatross human-powered aircraft.

The analyses, presented mainly in the Appendix, were done prior to flight tests and led to the following conclusions:

1. The estimated performance and trim computations show that this canard configuration, which requires a positive, tiltable canard lift vector to turn the airplane, can only be operated over a narrow range of speeds between the minimum power speed and that for which the canard trim lift is too small (for the Albatross, roughly 13 to 17 mph or 6 to 8 m/s).
2. The Gossamer aircraft have marginal or slightly negative pitch and yaw static stability, but large amounts of damping in pitch and roll, which somewhat compensates for the static instability.
3. Extremely light wing loading leads to a dominance of air apparent-mass effects on the effective heaving, rolling, and pitching inertias. These effects make the Gossamers very difficult to control in roll, and extremely sensitive to wind gust disturbances.
4. The most effective way of controlling roll is to use the tilting canard rudder to start a yawing motion whereby the rolling-moment-due-to-yawing (C_{ℓ_r}) effect creates a strong rolling moment.
5. The best turning maneuver is achieved by simultaneously tilting the canard to start a yawing motion toward the turn and warping the wings away from the turn, whereby the adverse yaw of the warped wings and C_{ℓ_r} effect helps to initiate the turn, while the warp restores a symmetric lift in the turn.

6. Stable lateral-directional control is achieved by continuous pilot action in tilting the canard rudder away from the low wing or in the direction of turn.

Using a sophisticated, lightweight instrumentation/telemetry/recording system provided by NASA-DFRC, good quality dynamic response measures were obtained for frequency sweep inputs to the elevator, wing warp, and canard rudder tilt. The conclusions are as follows:

1. The pitch rate response is essentially proportional to elevator deflection up to about 2 Hz (12 r/s), and fairly well matches the computed transfer function.
2. The normal acceleration response is contaminated by vibrations from the 2/revolution force pulsations of the propeller and by ambient gustiness during the flight tests.
3. The airspeed sensor response to elevator follows the computed transfer function reasonably well, when the latter is corrected for the sensor location and lag effects.
4. The roll- and yaw-rate responses to wing warp roughly follow the computed transfer functions but differ significantly in detail.
5. The roll- and yaw-rate responses to canard tilt are remarkably similar, and at the low frequencies used for control (below 1 Hz) can be characterized roughly as roll or yaw rate proportional to canard tilt angle delayed by .3 seconds. These measurements follow the computed transfer functions at moderate frequencies, but above about 1 Hz are higher in amplitude and lag more. These might be due to aeroelastic effects not included in the computations.
6. Coordinated turns were made using the technique described above, with fairly good coordination.
7. Attempts to more precisely verify apparent mass and roll inertia effects by dropping a 20-lb (9.1 kg) weight from one wing were not successful because

the step changes in roll rate and vertical acceleration were of the same order as the vibration effects from the propeller.

8. On two attempts to tow the aircraft without its propeller to measure performance parameters, a mildly unstable lateral-directional oscillation developed. This suggests that the towing airspeed may have been too high and that the propeller may have more stabilizing contribution than assumed.

Manual and automatic control of the Gossamer-type aircraft will be complicated by its three axes of slight instability and peculiar requirements for turn coordination, but the response properties are fairly benign and are easy to learn.

A number novel of and important aerodynamic, stability, and control phenomena are present in the Gossamer series of human-powered aircraft. The analyses and tests reported here showed considerable promise towards understanding them, but a number of areas deserve further research. These include:

- Better estimates of the pusher-propeller contributions to performance, stability, and control.
- Extraction of the key derivatives from the measured response data, which requires refined equations of motion and noise-tolerant estimation procedures.
- Improved estimates and wind-tunnel tests of the marginal static stability contributions. Especially needed are effective rotary derivatives, such as rolling-moment-due-to-yawing and -warp, yawing-moment-due-to-rolling and -warp (adverse yaw), damping in pitch, and the unsteady (apparent mass) effects of relative air-mass to vehicle accelerations.
- Further analysis and tests of gust response and closed-loop regulation are needed. Apparent mass and apparent inertial terms strongly influence the gust response and need to be better estimated and experimentally validated.

Building on the foundations given here, the above research should be very fruitful in extending the operational safety and altitudes of Gossamer-like aircraft of the future.

5. REFERENCES

1. MacCready, P.B., "Flight on 0.33 Horsepower: The Gossamer Condor," AIAA Paper 78-308, presented at AIAA 14th Annual Meeting, Washington, Feb. 1978.
2. Lissaman, P.B.S., H.R. Jex, and P.B. MacCready, "Stability and Control at Speeds Under 5 m/sec," Proc. of the Third Man-Powered Aircraft Group Symposium, London, England, Royal Aeronautical Society, Feb. 1978, pp. 83ff.
3. Burke, J.D., "The Gossamer Condor and Albatross: A Case Study in Aircraft Design," AeroVironment Inc. Report AV-R-80/540, June 1980 (also AIAA Professional Study Series).
4. Grosser, M., Gossamer Odyssey -- The Triumph of Human-Powered Flight, Boston, MA, Houghton-Mifflin, 1981.
5. MacCready, P.B., P.B.S. Lissaman, W.R. Morgan, and J.D. Burke, "Sun-Powered Aircraft Design," AIAA Paper 81-0916, presented at Annual Meeting and Technical Display, Long Beach, CA, May 1981.
6. Etkin, B., Dynamics of Flight, John Wiley & Sons, New York, NY, 1959.
7. McRuer, D., I. Ashkenas, and D. Graham, Aircraft Dynamics and Automatic Control, Princeton University Press, 1973.
8. Graham, D., and D. McRuer, Analysis of Nonlinear Control Systems, John Wiley & Sons, New York, NY, 1961 (also Dover, 1971).
9. McMasters, J., and G.M. Parker, "At the Threshold of Man-Powered Flight," Astronautics and Aeronautics, Sep. 1977, pp. 60-70.
10. MacCready, P.B., Gossamer Condor Planset, published by author (145 Vista Avenue, Pasadena, CA), 1978.
11. Moulton, R., "Gossamer Albatross -- Anatomy of a Cross-Channel Flyer," Flight International, Vol. 116, No. 3671, 28 July 1979, pp. 258-262.
12. Bateman, H., The Inertia Coefficients of an Airship in a Frictionless Fluid, NACA Report 164, 1923.
13. Liebeck, R.H., "Design of Airfoils for High Lift," in Evolution of Aircraft Wing Design Symposium, Proceedings of AIAA Conference, Dayton, OH, 1980, pp. 25ff.
14. Lissaman, P.B.S., "Wings for Human Powered Flight," in Evolution of Aircraft Wing Design Symposium, Proceedings of AIAA Conference, Dayton, OH, 1980, pp. 59ff.

15. Phillips, W.H., "Analysis of Effect of Asymmetrical Loading on Sailplane Performance in Circling Flight," in Motorless Flight Research, NASA CR-2315, 1973.
16. Magdaleno, R.E.: "The STI Frequency Domain Analysis Routine (FREDA)," STI WP-407-2, June, 1978.

APPENDIX

DYNAMIC STABILITY AND CONTROL ANALYSIS

This appendix summarizes the calculated stability and control properties of the flight-tested Gossamer Albatross and compares them with the earlier Gossamer Condor, with a reminder that most of the Condor calculations were originally made with various prototype versions having similar but not identical configurations. After presentation and discussion of the basic assumptions, aerodynamic dimensions, and acceleration terms (inertial and apparent masses), the aerodynamic coefficients are discussed. The resulting vehicle dynamic properties and flying qualities are then analyzed and discussed, with emphasis on the novel control scheme and complex dynamics involved in the turning maneuver.

A. Basic Assumptions and Parameters

1. Assumptions

A number of nonconventional features must be considered in calculating the dynamic response of the Gossamer aircraft, such as the canard elevator, pusher propeller, extremely low weight structure compared to the air-mass affected by the wing, and ground proximity effects. To obtain first approximations efficiently, a number of simplifying assumptions were made, following relatively crude justifications.

- i. Small-perturbation linearized equations are used, with the trim speeds of 16 ft/s (4.9 m/s)* for the Condor and 20 ft/s (6.1 m/s) and 28 ft/s (8.5 m/s) for the Albatross. The reference altitude is sea level.
- ii. Roughly symmetric flight is assumed so that the longitudinal and lateral-directional equations can be analyzed separately.

*Calculations were made in U.S. customary units and all results were converted to rounded SI units, given in parentheses for convenience only.

- iii. There are aerodynamic pressures caused by relative accelerations in all degrees of freedom between the air mass and airframe. These pressures give rise to the so-called "apparent-mass" tensor [e.g., see Ref. 12], and while it is usually negligible compared to the physical mass tensor for conventional aircraft, its effect often dominates the motions of the Gossamer aircraft. The low relative mass considerations are further discussed elsewhere in this appendix. Only the dominant apparent mass terms were actually used in these calculations (i.e., forces and moments from heaving, pitching, rolling, and yawing accelerations).
- iv. The propeller normal-force derivatives due to incidence and sideslip are neglected because it is in a "straightened" flow field behind the wing and fin-fuselage. The propeller/powerplant is operated at nearly constant power and efficiency, thereby causing the thrust changes to be inversely proportional to speed changes.
- v. Downwash and sidewash effects of the canard on the wing and fin are considered negligible, and likewise for the wing upwash on the canard. (The latter may not be as valid as the former.)
- vi. Aeroelastic effects are neglected. Because of the extensive wire bracing, the airframe is remarkably rigid in flight.
- vii. At the cruise height of about 5 to 15 feet (1.5 to 4.6 m), whereby the wing is 15 to 25 feet (4.6 to 7.6 m) above ground, the "reflection-plane" effects of the ground act to increase the lift-curve slopes by 5 to 10%, and thereby, increases slightly the surface effectiveness and reduces induced drag and downwash. For conservatism and simplicity, these ground-proximity effects were neglected in the stability analyses.

2. Parameters at Cruise

An updated set of key geometric dimensions has been compiled from authoritative sources and is presented in Table A-1. These may differ from those in various published

three-views, but they are compatible with the official Gossamer Condor plans [Ref. 10] and Albatross plans [Ref. 11], and are considered definitive.

The inertial parameters are summarized in Table A-2, which reveals that the gross weights of the aircraft are about one-third airframe and two-thirds payload (pilot power plant). The "apparent" masses and inertias are also shown in Table A-2. The air mass affected by airfoil motion was taken as a conical cylinder having, as its diameter, the surface chord for heave motions and its thickness for chordwise motions. An indication of the relative importance of apparent and inertial masses can be seen in the last column of Table A-2, where their ratio is tabulated. For example, for the Condor (Table A-2a), the effective mass in heave is nearly three times ($1 + 1.7 = 2.7$) the inertial mass, and the effective roll inertia is over five times the airframe moment of inertia. To put these effects into existing computer programs, the "effective inertias" were used in roll, pitch, and yaw; "pseudo- $\dot{\alpha}$ " (\dot{w} /airspeed) derivatives were used in heave, and the small surge and sway apparent mass effects were ignored.

Table A-3 gives several parameters related to the trim flight conditions. The aerodynamic stability derivatives at cruise were, in most cases, estimated by standard stability and control procedures, predominantly using NACA and RAE data summarized by Etkin [Ref. 6]. The resulting nondimensional parameters, included in Table A-3, are typical of high-aspect-ratio aircraft operating at high lift coefficients. The definitions of these parameters are standard [e.g., see Ref. 6 or 7]. A few of them deserve comment, however.

- i. The $C_{L\dot{\alpha}}$ and $C_{M\dot{\alpha}}$ terms are from the apparent mass effects (not downwash lags) and are put in this form to facilitate use in existing computer programs. They also were used for $\dot{\alpha}$ gust derivatives because the apparent mass terms derive from the relative acceleration between air and vehicle. Because $C_{M\dot{\alpha}}$ (actually $C_{M\dot{w}}$) is a small difference between the net moments of apparent inertia between the large canard and wing terms, it is negative for the Condor and positive for the Albatross.

- ii. The thrust/speed and thrust/power sensitivities are dimensional and assume constant power operation. Here, the "throttle" control is input power, $\delta_{hp} = thp/\eta_p$.
- iii. C_{M_α} is slightly unstable for all but the Albatross high-speed condition.
- iv. There is essentially no weathercock stability. The very low $C_{n\beta}$ results from small and uncertain unstable fin-fuselage effects and slightly stable wing effects. The slightly stabilizing effects of the aft propeller were neglected because it operates in the fuselage/wing downwash and side-wash.
- v. The wing warp "aileron" derivatives were estimated using the analogy between an untwisted rolling wing and a linearly-twisted nonrolling wing. Hence, the rolling effectiveness is $C_{l_{\delta_w}} = -C_{l_p}$ and the adverse yaw is $C_{n_{\delta_w}} = +C_{n_p}$, where δ_w is the twist angle at each wing tip (assuming equal and opposite deflections), and positive for right wing down. The value for C_{n_p} is difficult to estimate confidently for wings at high lift coefficient and low Reynolds number (as here), because there are opposing effects of the induced drag and profile drag terms. For these Stratford-recovery airfoils, there is evidence that the profile drag remains fairly constant up to stall; hence, the adverse yaw effects of the induced drag variations should predominate.
- vi. The canard tilt "rudder" derivatives assume that a constant lift vector is rotated through the small tilt angle, δ_r , thereby producing a side force at the canard location.

$$C_{y\delta_r} = C_{L_c} (S_c/S) \quad (A-1)$$

$$C_{n\delta_r} = C_{y\delta_r} (l_c/b) \quad (A-2)$$

$$C_{l_{\delta_r}} = 0 \quad (A-3)$$

B. Longitudinal Dynamics

1. Equations

The resulting dimensional longitudinal equations of motion for perturbations of inertial speed, u ; vertical velocity, w ; and pitch angle, θ , put in standard Laplace-operator form, are given in Table A-4. Generally, these equations have been divided through by the effective mass or inertia so that these dimensional coefficients represent actual linear or rotary accelerations due to the applied variable [e.g., see Ref. 7]. Exceptions exist for the heave equations, where the true mass is used and the apparent mass effects show up as Z_w and M_w terms. The gust terms, which are complex, have been omitted from this presentation. The gust response of such a light aircraft is strongly affected by apparent mass effects and will not be analyzed here.

The numerical coefficients of the equations are given in matrix format in Table A-4b. The values are in U.S. customary units of ft/s^2 for translations, and rad/s^2 for rotations. Thus, the rotational equations are the same in both unit systems, while the translational equations (i.e., for u , v , or w perturbations) can simply be divided by 3.28 (ft/m) for use with SI-unit perturbations.

2. Dynamic Properties

These equations were solved for the transfer functions relating various motions of interest to each of the inputs. The longitudinal transfer functions are given in Table A-5.

A number of interesting dynamic properties are revealed by these transfer functions. For conventional aircraft, the characteristic polynomial, Δ_{long} , usually reflects two second-order modes: the low speed "phugoid" mode (in which angle of attack is nearly constant) and the "short-period" mode dominated by the static (weathervane) stability, $C_{m\alpha}$. In contrast, only the Albatross at high speed has a second-order mode; otherwise, both aircraft have all first-order modes, which are highly coupled and bear little resemblance to the classical modes. Among the complicating factors are: the small static instability, the very large pitch and heave damping (M_q and Z_w , respectively), the strong variation of thrust and its pitching moment with airspeed, and large apparent-mass

and inertia terms. In effect, the longitudinal dynamics are dominated by a free integrator and a pair of first-order lags having time constants on the order of 1/2 second. Such dynamics are relatively easy to control in pitch and lead to very "docile" flying qualities.

As can be seen by comparing values in Table A-5, the elevator-to-pitch numerator, $N_{\delta_e}^\theta$, has a pair of first-order zeros near the denominator's mid-pair of dominant poles, but their values are not always related to the conventional aircraft ($1/T_{\theta_1}$ and $1/T_{\theta_2}$) zeros. They serve to cancel most of the lag effects and make the Condor's pitch response appear to the pilot as a nearly pure pitch-rate control.

It can be shown that even a very low gain pitch-attitude stabilization control by the pilot completely stabilizes the low frequency mode and gives very stable first-order closed-loop modes at about 1 to 2 rad/s. Theoretically, this type of K/s-like "inner loop" makes all other longitudinal degrees of freedom easy to control, and this has been verified by the pilot.

3. Approximate Pitch Dynamics

Some insight and a useful approximation to the pitch control dynamics results from the near-perfect cancellation of $1/T_{p_2}$ by $1/T_{\theta_1}$, and $1/T_{sp_1}$ by $1/T_{\theta_2}$, in Table A-5. Letting the small $1/T_{p_1}$ equal 0, the approximate pitch rate response to canard elevator deflection is:

$$\frac{\dot{\theta}}{\delta_e} = s \frac{N_{\delta_e}^\theta}{\Delta_{\text{long}}} \doteq \frac{s M_{\delta_e}}{s(s - M_q)} = \frac{M_{\delta_e}}{(s - M_q)} \quad (\text{A-4})$$

In even simpler terms, write this in Bode format, and note that nearly all pitch damping, M_q , and elevator effectiveness, M_{δ_e} , are due to the canard surface itself. The resulting expression is:

$$\frac{\dot{\theta}}{\delta_e} = \frac{M_{\delta_e}/M_q}{\left(\frac{s}{-M_q} + 1\right)} \cong \frac{(U_o/l)}{\left(\frac{s}{-M_q} + 1\right)} \quad (\text{A-5})$$

where

$$l = \text{elevator arm } (-l_c) \text{ or effective arm } (l_w - l_c) \quad (\text{A-5a})$$

$$M_q = \rho U_o S_c l C_{L\alpha_c} / 2I_{y_{\text{eff}}} \quad (\text{A-5b})$$

This expression says that the ratio of pitch rate to canard deflection corresponds to the ratio (flight speed/canard moment arm) up to a frequency of $-M_q$ (rad/s); here, about 6 to 10 rad/s or 1 to 1.5 Hz (time constant of 0.6 to 1.0 seconds).

This sort of response is like that of an automobile at low speeds, where the yaw rate response from a steer angle is proportional to the ratio (speed wheel base). The equivalent to the wheel base would be the canard moment arm $(-l_c)$ or, more correctly, the canard to quarter-MAC distance, $l_{\text{eff}} = l_w - l_c$ (canard arm is negative). For the computed cases, the results compare as follows:

Speed	Condor 16 ft/s	Albatross-II 20 ft/s	28 ft/s	
Exact $\frac{\dot{\theta}}{\delta_e} \approx$	$\frac{.52}{\frac{s}{6.14} + 1}$	$\frac{.79}{\frac{s}{7.16} + 1}$	$\frac{1.10}{\frac{s}{9.56} + 1}$	$\left[\frac{\text{deg/s}}{\text{deg}} \right] \quad (\text{A-6})$

(a) Approximate: Equation (A-5) with $(-l_c)$

$\frac{.82}{\frac{s}{6.14} + 1}$	$\frac{.89}{\frac{s}{7.16} + 1}$	$\frac{1.24}{\frac{s}{10.15} + 1}$	(A-7)
----------------------------------	----------------------------------	------------------------------------	----------------

(b) Approximate: Equation (A-5) with $(l_w - l_c)$

$\frac{.76}{\frac{s}{6.14} + 1}$	$\frac{.83}{\frac{s}{7.16} + 1}$	$\frac{1.16}{\frac{s}{10.15} + 1}$	(A-8)
----------------------------------	----------------------------------	------------------------------------	----------------

The last expression closely approximates the detailed computations in all cases and can be used to quickly estimate the pitch attitude dynamics of the Gossamer-type designs (where the static margin is very small).

C. Lateral Directional Dynamics

1. Equations and Open-Loop Responses

As explained in the earlier portion of this report, roll and turn control is a major problem for human-powered aircraft. Large rolling moments would not roll the aircraft very rapidly. This was traced via analysis to the large apparent moment of inertia in roll, which is over five times the airframe inertia. Conversely, yawing rates produced rolling mainly through the strong $C_{\ell r}$ effects. Early analyses revealed the futility of conventional ailerons for roll control, the need for some fin area to enhance $C_{y\beta}$ and $C_{n\beta}$, and the seeming paradox that twisting the wings for a leftward rolling moment would quickly yield a yawing velocity and roll angle to the right [Ref. 4].

This effect of "adverse yaw" is shown in the open-loop, transient response of the Condor in Figure A-1, calculated via the S.T.I. "USAM" computer program using the equations of Table A-6b and A-6c. Warping the wings for a left-wing-down rolling moment immediately creates a large nose-right "adverse yaw" torque of about 15% of the rolling torque. Because the effective inertia in yaw is less than one-fifth of that in roll and the weathervane stability is small, the airframe immediately starts to yaw right. The strong rolling moment from yawing, $C_{\ell r} \cdot r$ (due to the outside wing moving faster than the inside wing), quickly overpowers the $C_{\ell \delta_w} \cdot \delta_w$ (warp effect), so the aircraft starts to roll right within about two seconds. The nose-right adverse yaw also creates, initially, a negative sideslip, β (wind from the left), but this soon changes to a positive sideslip (into the turn) after about eight seconds. The original calculations suggested, and the recent calculations validated, the use of this adverse yaw effect to aid in both initiating and trimming the turns.

The open loop response of the Condor to a 1.0 degree nose-right tilt of the canard rudder is given in Figure A-2. It can be seen that the yaw rate builds up within a couple of seconds, thereby rolling the aircraft right-wing-down due to the strong $C_{\ell r} \cdot r$ effect.

The result is an overbanked turn in which a positive (rightward) sideslip develops; nevertheless, the dihedral effect is not sufficient to stop the rolling. The important point to remember here is that the canard-tilt rudder acts as a more powerful and rapid roll rate control than wing warp, while the wing warp acts as a better yaw rate initiator than the canard, by a factor of about 5:1. We will later discuss the combination of these unusual effects to give an effectively coordinated (zero-sideslip) turn.

2. Transfer Functions and Dynamics

The lateral transfer function dynamics are tabulated in Table A-7. First, consider the characteristic equation:

$$\begin{array}{l} \text{Condor: } \Delta_{\text{lat}} = (s + .0098) (s + .829) \left[s^2 + 2 (.84) (3.35) s + 3.35^2 \right] \\ \text{Albatross: } \Delta_{\text{lat}} = (s - .023) (s + 4.28) \left[s^2 + 2 (.93) (1.80) s + 1.80^2 \right] \end{array}$$

Although this has two real roots similar to conventional "spiral" and "roll-subsidence" modes, and two very well-damped oscillatory roots similar to conventional "Dutch-roll" modes, three of these are not at all similar in properties to the conventional modes.

Only the spiral mode is conventional; it is dominated by a moderate dihedral effect, weak yaw damping (due mainly to wing and wire drag), strong rolling moment due to yawing, and very weak and uncertain directional stability (slightly unstable fin-fuselage; slightly stable wing). The " $1/T_R$ " root is not well approximated by the roll damping coefficient of L_P , as it is for a conventional aircraft but is, instead, related also to the sideslip damping, Y_v ; nor is $\omega_D^2 \approx N_\beta$, as it is for a conventional "Dutch-roll" mode. This oscillatory mode should more properly be termed the "wallowing" mode, as it involves a sequence of well-damped yawing and rolling motions unlike normal weathervane yaw modes.

The transfer function numerator relating roll angle to "aileron" (wing warp) (ϕ/δ_w) has a negative root (it is in the right-half s-plane, a so-called "nonminimum phase" zero). This implies that the steady-state roll rate has the opposite sign from the initial roll rate, as previous examination of Figure A-1 disclosed. Because of this effect, closed-loop roll control by wing warp is not satisfactory, although the warp provides a very low drag roll trim via a linear redistribution of the local angle of attack to compensate for the linear velocity gradient due to yawing. This is the optimum twist for an elliptical planform [Ref. 15].

On the other hand, the tilting canard rudder roll transfer function, $N_{\delta_r}^{\phi}/\Delta_{lat}$, has good properties for closed loop control of roll angle by tilting the canard opposite to bank angle error (e.g., just holding the canard level with the horizon will provide a low gain roll stabilization loop). Further details of such closed loop dynamics are given elsewhere [Ref. 2] and are beyond the scope of this report.

3. Turning Maneuvers

The turn entry response for a closed-loop 2-degree banked turn command is shown in Figure A-3 for the Condor. The required control action, $\delta_r(t)$ is, roughly, a 10-degree lift-tilt "pulse" for about one to two seconds to initiate a suitable yaw rate, followed by a gradually decreasing control as the wing is brought and held to a 2-degree right bank in a few seconds. Meanwhile, the sideslip grows to about 5 degrees towards the turn center so that the dihedral effect ($L_{\beta} \cdot \beta$) fights the excessive ($L_r \cdot r$) term, while ($U_o Y_v \cdot \beta$) fights the banked wing's side force. The resulting turn rate of about 1.5 degrees per second is much less than the ideal value of about 4.02 degrees per second for a true coordinated turn of about 230 feet (70 m) radius at 16 ft/s (4.9 m/s) ($\dot{\lambda}_{ideal} = g\phi/U_o$). It is interesting to note that such a turn radius is only a 2.4-span difference, whereby $(rb/2U_o) = .21$, so the outside wing tip is traveling 21% faster than the centerline, while the left wing is moving 21% slower than the centerline [see Ref. 15 for a discussion of these points].

This problem is relieved when the wing warp is stepped -4.1 degrees to the left for a right turn of 2 degrees bank. This ratio (-2.05 degrees of opposite aileron for each degree of desired bank angle) was computed from the closed loop system sensitivities to give a coordinated turn; i.e., zero sideslip. That $\beta = 0$ is achieved within about 10 seconds is

seen in Figure A-3. However, this high yaw rate of about 3 degrees per second tends to overbank the aircraft, so the canard rudder has to be tilted out of the turn several degrees. This opposes, somewhat, the centrifugal force from the banked wing and reduces the turn rate from its ideal value of 4 degrees per second to about 3 degrees per second. This is the turn coordinate scheme used on the Gossamer series of aircraft, and the flight experience is reasonably well-matched by these analytical results.

TABLE A-1a. Key Aerodynamic Dimensions for Gossamer Condor (1977).

Parameter	Symbol	Units	Wing	Canard	Fuselage	Propeller
Area	S	ft ² (m ²)	712.5 (66.3)	88.8 (8.3)	85.5 (7.9)	7.0 projected (.6)
Span	b	ft (m)	96 (29.28)	22.3 (6.80)	9.0 (2.75)	12.7 diameter (3.87)
Aspect Ratio	AR	--	12.9	5.60	0.95 (geom.) 1.9 (eff.)	4.6 (1 blade) 6.0 (eff.)
Taper Ratio	λ	--	.5	1.0	1.4	1.0
Thickness ratio	τ	--	.11	.11	.18	.12
Sweep at $c/4$	Λ	degrees	9	0	1	0
Dihedral	Γ	degrees	3	0	--	--
Chord aerodynamic	\bar{c}	ft (m)	7.78 (2.37)	4.2 (1.28)	9.2 (2.81)	1.25 (.38)
$\bar{c}/4$ distances (+ = aft of CG)	l	ft (m)	+1.5 (+.46)	-19.5 (-5.95)	-1.0 (-.31)	+8.5 (+2.59)
Incidence (cruise)	i	degrees	5	6 (est.)	0	--

TABLE A-1b. Key Aerodynamic Dimensions for Gossamer Albatross II (1980 tests).

Parameter	Symbol	Units	Wing	Canard	Fuselage	Propeller
Area	S	ft ² (m ²)	488 (45.3)	64.2 (6.0)	70.4 (6.5)	6.7 projected (.6)
Span	b	ft (m)	96.0 (29.26)	18.3 (5.58)	9.5 (2.90)	13.5 diameter (4.11)
Aspect Ratio	AR	--	18.9	5.2	1.3 (geom.) 1.8 (eff.)	13.4 (1 blade) 6.0 (eff.)
Taper Ratio (Outer Panel) (Effective)	λ	--	.71 (outer) .85 (eff.)	1.0	.91	.4
Thickness ratio	τ	--	.11	.11	.13	.11
Sweep at c/4	Λ	degrees	7.0	0	-4	0
Dihedral	Γ	degrees	3.6	0	--	--
Chord aerodynamic	\bar{c}	ft (m)	5.17 (1.58)	3.50 (1.07)	7.85 (2.39)	.80 (.24) at .75R
$\bar{c}/4$ distances (+ = aft of CG)	ℓ	ft (m)	+1.67 (+.51)	-22.5 (-6.86)	0 (-0)	+8.0 (+2.44)
Chord Plane Incidence at cruise	i	degrees	4	6 (est.)	-1.6 ref (boom)	--

TABLE A-2a. Inertial Parameters for Gossamer Condor (1977).

Name	Symbol	Units	Aircraft	+ Pilot	= Total	
Weight	W	lbs (kg)	71 (32)	+ 141 (64)	= 212 (96)	
<u>Masses:</u>			Aircraft	Air, Apparent (main surfaces)	Effective	<u>Apparent Inertia</u>
			m	m _a	m _e	m _a /m
Surge	M _x	Slug (kg)	6.6 (96)	0.14 (2.0)	6.7 (98)	.02
Sway	M _y	Slug (kg)	6.6 (96)	1.40 (20)	8.0 (116)	.21
Heave	M _z	Slug (kg)	6.6 (96)	11.2 (164)	17.1 (260)	1.70
<u>Inertias:</u>			I	I _a	I _e	I _a /I
Roll	I _x	Slug ft ² (kg m ²)	1240 (1682)	5491 (7451)	6731 (9134)	4.4
Pitch	I _y	Slug ft ² (kg m ²)	270 (366)	398 (540)	668 (906)	1.4
Yaw	I _z	Slug ft ² (kg m ²)	1250 (1696)	66 (207)	1316 (1786)	.09

TABLE A-2b. Inertial Parameters for Gossamer Albatross II (1980 tests).

Name	Symbol	Units	Aircraft	+ Pilot	+ Instrumentation, Electric Drive	= Total
Weight	W	lbs (kg)	64 (29)	+ 141 (64)	+ 17 (8)	= 222 (101)
<u>Masses:</u>			Aircraft	Air, Apparent (main surfaces)	Effective	<u>Apparent Inertia</u>
			m	m _a	m _e	m _a /m
Surge	M _x	Slug (kg)	6.9 (101)	0.07 (1.0)	7.0 (102)	.01
Sway	M _y	Slug (kg)	6.9 (101)	1.1 (16)	8.0 (117)	.16
Heave	M _z	Slug (kg)	6.9 (101)	5.0 (73)	11.9 (174)	.72
<u>Inertias:</u>			I	I _a	I _e	I _a /I
Roll	I _x	Slug ft ² (kg m ²)	779 (1057)	3524 (4780)	4303 (5837)	4.5
Pitch	I _y	Slug ft ² (kg m ²)	163 (221)	226 (307)	389 (528)	1.4
Yaw	I _z	Slug ft ² (kg m ²)	778 (1055)	47 (64)	815 (1119)	.06

TABLE A-3. Trim Conditions and Nondimensional Aerodynamic Derivatives at Cruise.

Item	Units	Condor (1977)	Albatross II (1980)	
			Standard Condition	High Speed
A. Trim Conditions				
Altitude	ft	sea level	sea level	sea level
Airspeed	ft/s (m/s)	16 (4.9)	20 (6.1)	28 (8.5)
Dynamic Pressure	lb/ft ² (N/m ²)	.304 (14.6)	.476 (22.9)	.932 (44.8)
Lift	lb (N)	212 (944)	222 (988)	222 (988)
Drag	lb (N)	9.7 (43)	8.0 (36)	9.1 (41)
Lift/Drag	--	22	28	24
Static Margin	$\Delta X_{ac}/\bar{c}$	-.045	-.16	+.002
Maneuver Margin	$\Delta X_{mc}/\bar{c}$	4.95	--	--
B. Longitudinal Derivatives (Out of Ground Effect)				
C_L	--	1.00	0.96	0.49
$C_{L\alpha}$	1/rad	5.40	5.58	6.15
$C_{L\dot{\alpha}}$ (apparent mass)	1/rad	3.38	3.35	3.35
C_D	--	.0452	.0344	.0201
$C_{D\alpha}$	1/rad	0.061	0.045	0.021
$C_{m\alpha}$	1/rad	0.240	0.170	-0.010
C_{mq}	1/rad	-10.0	-18.08	-18.20
$C_{m\dot{\alpha}}$ (apparent mass)	1/rad	-.85	.23	.23
$C_{L\delta_e}$ (canard elevator)	1/rad	.66	.42	.42
$C_{D\delta_e}$ (canard elevator)	1/rad	0	.010	.003
$C_{m\delta_e}$ (canard elevator)	1/rad	1.26	1.84	1.84
$\partial T/\partial u$ (at .3 horsepower)	lb/ft/s (N/m/s)	-.60 (-8.8)	-.40 (-5.9)	-.32 (-4.7)
$\partial T/\partial hp$	lb/hp (N/W)	43 (.257)	22 (.131)	15.7 (.094)

TABLE A-3. (continued)

Item	Units	Condor (1977)	Albatross II (1980)	
			Standard Condition	High Speed
C. Lateral Directional Derivatives (Body - Fixed Stability Axis System)				
$C_{y\beta}$	1/rad	-.28	-.28	-.28
$C_{l\beta}$	1/rad	-.104	-.145	-.124
C_{lp}	1/rad	-.56	-.55	-.61
C_{lr}	1/rad	.250	.164	.122
$C_{n\beta}$	1/rad	-.0050	.0079	.0022
C_{np}	1/rad	-.080	-.089	-.047
C_{nr}	1/rad	-.0150	-.0048	-.0048
$C_{y\delta_w}$ (per side)	1/rad	0	0	0
$C_{l\delta_w}$ (per side)	1/rad	.56	.55	.61
$C_{n\delta_w}$ (per side)	1/rad	-.080	-.089	-.047
$C_{y\delta_r}$	1/rad	.083	.065	.022
$C_{l\delta_r}$	1/rad	0	0	0
$C_{n\delta_r}$	1/rad	.0340	.0152	.0052

TABLE A-4. Longitudinal Equations of Motion.

a. Equations

Surge:

$$(s - X_u^*) u - X_w w + g \theta = X_{\delta_e} \delta_e + X_{\delta_{hp}} \delta_{hp}$$

Heave:

$$-Z_u^* u + [(1 - Z_w^*) s - Z_w] w - U_o s \theta = Z_{\delta_e} \delta_e + Z_{\delta_{hp}} \delta_{hp}$$

Pitch:

$$M_u^* u - (M_w s + M_w) w + (s^2 - M_q s) \theta = M_{\delta_e} \delta_e + M_{\delta_{hp}} \delta_{hp}$$

b. Numerical Matrices (in standard matrix form and U.S. customary units)

1. Condor (1977); $U_o = 16 \text{ ft/s (4.9 m/s)}$

$$\begin{bmatrix} (s + .276) & -1.93 & 32.2 \\ +4.10 & (2.70s + 11.2) & -16s \\ .0137 & (+.0326s - .0379) & (s^2 + 6.14s) \end{bmatrix} \cdot \begin{bmatrix} u \\ w \\ \theta \end{bmatrix} = \begin{bmatrix} 0 & 6.50 \\ -21.7 & -.569 \\ 3.18 & .322 \end{bmatrix} \cdot \begin{bmatrix} \delta_e \\ \delta_{hp} \end{bmatrix}$$

2. Albatross II (1980); $U_o = 20 \text{ ft/s (6.1 m/s)}$

$$\begin{bmatrix} (s + .173) & -1.54 & 32.2 \\ 3.22 & (1.73s + 9.4) & -20 s \\ .0108 & (-.0046s - .0262) & (s^2 + 7.16s) \end{bmatrix} \cdot \begin{bmatrix} u \\ w \\ \theta \end{bmatrix} = \begin{bmatrix} -.336 & 3.17 \\ -14.1 & -.300 \\ 5.67 & -.198 \end{bmatrix} \cdot \begin{bmatrix} \delta_e \\ \delta_{hp} \end{bmatrix}$$

3. Albatross II (1980); $U_o = 28 \text{ ft/s (8.5 m/s)}$

$$\begin{bmatrix} (s + .142) & -1.10 & 32.2 \\ 2.30 & (1.73s + 14.5) & -28s \\ .0088 & (-.0046s + .0022) & (s^2 + 10.15s) \end{bmatrix} \cdot \begin{bmatrix} u \\ w \\ \theta \end{bmatrix} = \begin{bmatrix} -.198 & 2.27 \\ -27.7 & -.099 \\ 11.2 & -.141 \end{bmatrix} \cdot \begin{bmatrix} \delta_e \\ \delta_{hp} \end{bmatrix}$$

TABLE A-5. Longitudinal Transfer Functions.

Transfer Function	Term	Condor (1978)	Albatross II (1980)	
		$U_o = 16 \text{ ft/s}$ (4.9 m/s)	$U_o = 20 \text{ ft/s}$ (6.1 m/s)	$U_o = 28 \text{ ft/s}$ (8.5 m/s)
Δ	$1/T_{p_1} (\zeta_p)$	-.00094	.0122	(.918)
	$1/T_{p_2} (\omega_p)$	1.74	.772	(.172)
	$1/T_{sp_1}$	2.26	4.85	8.75
	$1/T_{sp_2}$	6.74	7.16	9.56
	D.C. gain	-.025	.327	2.48
$N_{\delta_e}^\theta$	A_θ	3.44	5.64	11.05
	$1/T_{\theta_1}$	1.41	.79	.32
	$1/T_{\theta_2}$	2.62	4.85	8.28
	D.C. gain	12.71	21.5	29.4
$N_{\delta_e}^\alpha$	A_α	-.504	-.409	-.572
	$1/T$	-1.72	-3.79	-3.49
	ζ_α	.87	.46	.433
	ω_α	3.32	3.30	2.91
	D.C. gain	-9.56	16.9	16.9
$N_{\delta_e}^h$	A_h	-8.07	-22.8	-44.7
	$1/T_{h_1}$.243	.175	.139
	$1/T_{h_2}$	3.78	-3.59	(-5.43)
	$1/T_{h_3}$	6.87	6.39	10.4
	D.C. gain	50.9	91.5	351.

TABLE A-5. (continued)

Transfer Function	Term	Condor (1978)	Albatross II (1980)	
		$U_o = 16 \text{ ft/s}$ (4.9 m/s)	$U_o = 20 \text{ ft/s}$ (6.1 m/s)	$U_o = 28 \text{ ft/s}$ (8.5 m/s)
$N_{\delta_{np}}^h$	A_h	.211	1.27	.836
	$1/T_{h1}$	-.118	-.100	10.4
	$1/T_{h2}$ (ξ_h)	6.81	3.54	(-.438)
	$1/T_{h3}$ (ω_h)	31.9	5.75	(.222)
	D.C. gain	-5.41	-2.59	.428
$N_{\delta_e}^u$	A_u	-15.6	-.336	-.198
	$1/T_{u1}$	3.71	37.5	90.
	ξ_u ($1/T_{u2}$)	(7.20)	.706	.691
	ω_u	—	8.87	13.0
	D.C. gain	-417.	-991.	-3010.

TABLE A-6. Lateral-Directional Equations of Motion.

a. Equations

$$\begin{array}{rcllcl}
 (s - Y_v)\beta & + & r - (g/U_o)\phi & = & Y_{\delta_w}^* \delta_w & + Y_{\delta_r}^* \delta_r \\
 -L_\beta \beta + (s + L_p) p - L_r r & & & = & L_{\delta_w} \delta_w & + L_{\delta_r} \delta_r \\
 -N_\beta \beta - N_p p + (s - N_r) r & & & = & N_{\delta_w} \delta_w & + N_{\delta_r} \delta_r \\
 & - p & + & s\phi & = & 0 \\
 -s\beta & & -r & + & \dot{\lambda} & = & 0
 \end{array}$$

b. Numerical Matrices (in standard matrix form and U.S. customary units).

1. Condor; $U_o = 16 \text{ ft/s (4.9 m/s)}$

$$\begin{bmatrix}
 (s + .576) & 0 & +1.0 & +2.01 & 0 \\
 +.32 & (s + 5.19) & -2.32 & 0 & 0 \\
 -.079 & +3.79 & (s + .712) & 0 & 0 \\
 0 & -1 & 0 & s & 0 \\
 -s & 0 & -1 & 0 & +1
 \end{bmatrix} \cdot \begin{bmatrix} \beta \\ p \\ r \\ \phi \\ \dot{\lambda} \end{bmatrix} = \begin{bmatrix} 0 & .171 \\ +1.73 & 0 \\ -1.27 & +.538 \\ 0 & 0 \\ 0 & 0 \end{bmatrix} \cdot \begin{bmatrix} \delta_w \\ \delta_r \end{bmatrix}$$

TABLE A-6 (continued).

2. Albatross; $U_0 = 20$ ft/s (6.1 m/s)

$$\begin{bmatrix} (s + .471) & 0 & +1.0 & +1.61 & 0 \\ +.75 & (s + 6.83) & -2.04 & 0 & 0 \\ -.213 & +5.77 & (s + .311) & 0 & 0 \\ 0 & -1 & 0 & s & 0 \\ -s & 0 & -1 & 0 & +1 \end{bmatrix} \cdot \begin{bmatrix} \beta \\ p \\ r \\ \phi \\ \dot{\lambda} \end{bmatrix} = \begin{bmatrix} 0 & .109 \\ 2.85 & 0 \\ -2.40 & .410 \\ 0 & 0 \\ 0 & 0 \end{bmatrix} \cdot \begin{bmatrix} \delta_w \\ \delta_r \end{bmatrix}$$

3. Albatross II (1980); $U_0 = 28$ ft/s (8.5 m/s)

$$\begin{bmatrix} (s + .659) & 0 & +1.0 & +1.15 & 0 \\ +1.26 & (s + 10.6) & -2.12 & 0 & 0 \\ -.116 & +4.26 & (s + .435) & 0 & 0 \\ 0 & -1 & 0 & s & 0 \\ -s & 0 & -1 & 0 & +1 \end{bmatrix} \cdot \begin{bmatrix} \beta \\ p \\ r \\ \phi \\ \dot{\lambda} \end{bmatrix} = \begin{bmatrix} 0 & .052 \\ 6.19 & 0 \\ -2.49 & .275 \\ 0 & 0 \\ 0 & 0 \end{bmatrix} \cdot \begin{bmatrix} \delta_w \\ \delta_r \end{bmatrix}$$

TABLE A-7. Lateral-Directional Transfer Functions.

Transfer Function	Term	Condor (1977)	Albatross II (1980)	
		$U_o = 16 \text{ ft/s}$ (4.9 m/s)	$U_o = 20 \text{ ft/s}$ (6.1 m/s)	$U_o = 28 \text{ ft/s}$ (8.5 m/s)
Δ	$1/T_S$.0098	-.023	.021
	$1/T_R$.829	4.28	9.72
	ζ_D	.84	.93	.75
	ω_D	3.35	1.80	1.31
	D.C. gain	.091	-.324	.346
$N_{\delta_w}^{\phi}$	A_{ϕ}	1.73	2.85	6.19
	$1/T_{\phi_1}$.67	.67	.945
	$1/T_{\phi_2}$	-1.07	-1.61	-.703
	D.C. gain	-1.25	-3.08	-4.11
$N_{\delta_w}^r$	A_r	-1.27	-2.40	-2.49
	$1/T_{r_1}$.085	13.7	.093
	$1/T_{r_2} (\zeta_r)$.487	(.96)	.563
	$1/T_{r_3} (\omega_r)$	10.4	(.242)	21.2
	D.C. gain	-.543	-1.93	-2.77
$N_{\delta_w}^{\beta}$	A_{β}	1.27	2.40	2.49
	$1/T_{\beta_1}$	-.203	-.171	-.050
	$1/T_{\beta_2}$	13.3	15.7	24.1
	D.C. gain	-3.42	-6.45	-2.97

TABLE A-7. (continued)

Transfer Function	Term	Condor (1977)	Albatross II (1980)	
		$U_o = 16 \text{ ft/s}$ (4.9 m/s)	$U_o = 20 \text{ ft/s}$ (6.1 m/s)	$U_o = 28 \text{ ft/s}$ (8.5 m/s)
$N_{\delta_w}^\lambda$	A_λ	2.76	3.45	5.48
	$1/T_{\lambda_1}$.049	.087	.073
	$1/T_{\lambda_2}$	-4.04	-6.43	-6.96
	D.C. gain	-5.43	-1.93	-2.77
$N_{\delta_r}^\phi$	A_ϕ	1.19	.754	.519
	$1/T_\phi$.741	.960	1.38
	D.C. gain	.883	.723	.715
$N_{\delta_r}^r$	A_r	.538	.410	.275
	$1/T_{r_1}$	5.14	6.67	.282
	$1/T_{r_2} (\xi_r)$	(.93)	(.806)	.487
	$1/T_{r_3} (\omega_r)$	(.355)	(.425)	10.5
	D.C. gain	.348	.496	.398
$N_{\delta_r}^\beta$	A_β	.171	.109	.052
	$1/T_{\beta_1}$	4.40	5.79	-3.18
	$1/T_{\beta_2} (\xi_\beta)$	(-.45)	(-.824)	-4.04
	$1/T_{\beta_3} (\omega_\beta)$	(1.83)	(1.46)	10.1
	D.C. gain	2.51	1.35	.671

TABLE A-7. (continued)

Transfer Function	Term	Condor (1977)	Albatross II (1980)	
		$U_o = 16 \text{ ft/s}$ (4.9 m/s)	$U_o = 20 \text{ ft/s}$ (6.1 m/s)	$U_o = 28 \text{ ft/s}$ (8.5 m/s)
$N_{\delta_r}^{\lambda}$	A_{λ}	.171	.109	.052
	$1/T_{\lambda_1}$.083	.163	.141
	$1/T_{\lambda_2}$	3.87	5.17	9.87
	λ_{ξ}	.39	.39	.22
	λ_{ω}	2.52	2.32	2.35
	D.C. gain	.348	.496	.398

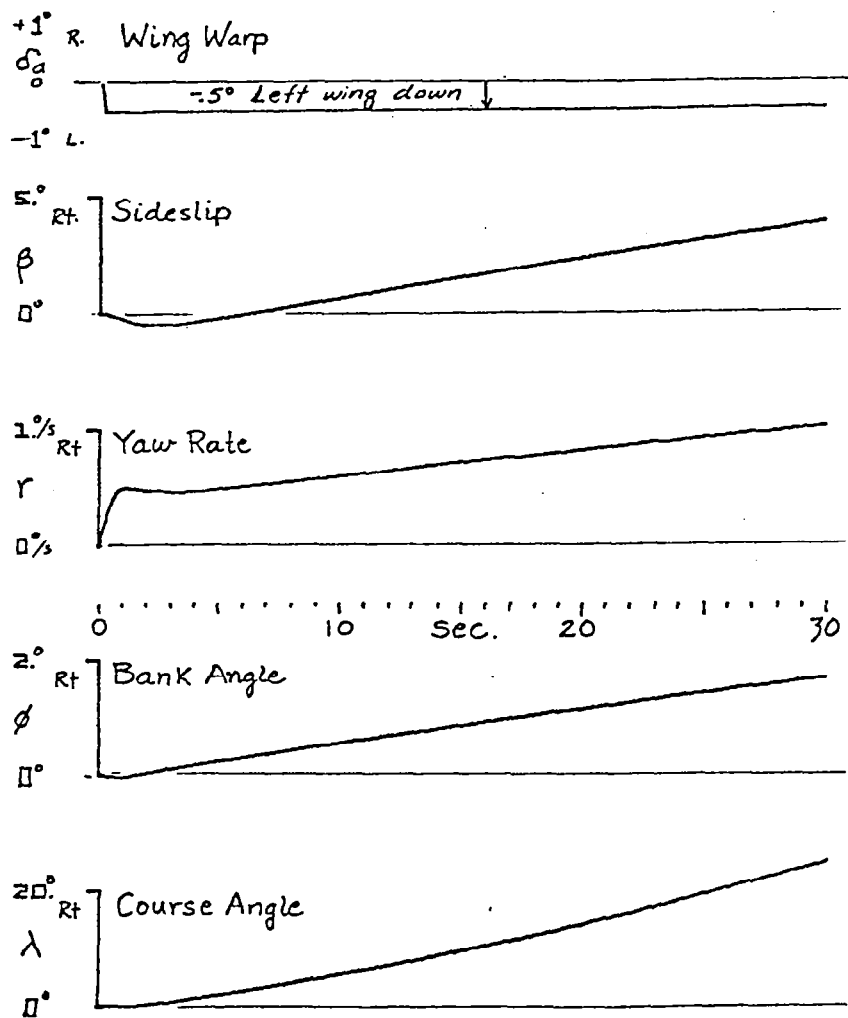


Figure A-1. Transient Response of Gossamer Condor to a Leftward Wing Warp.

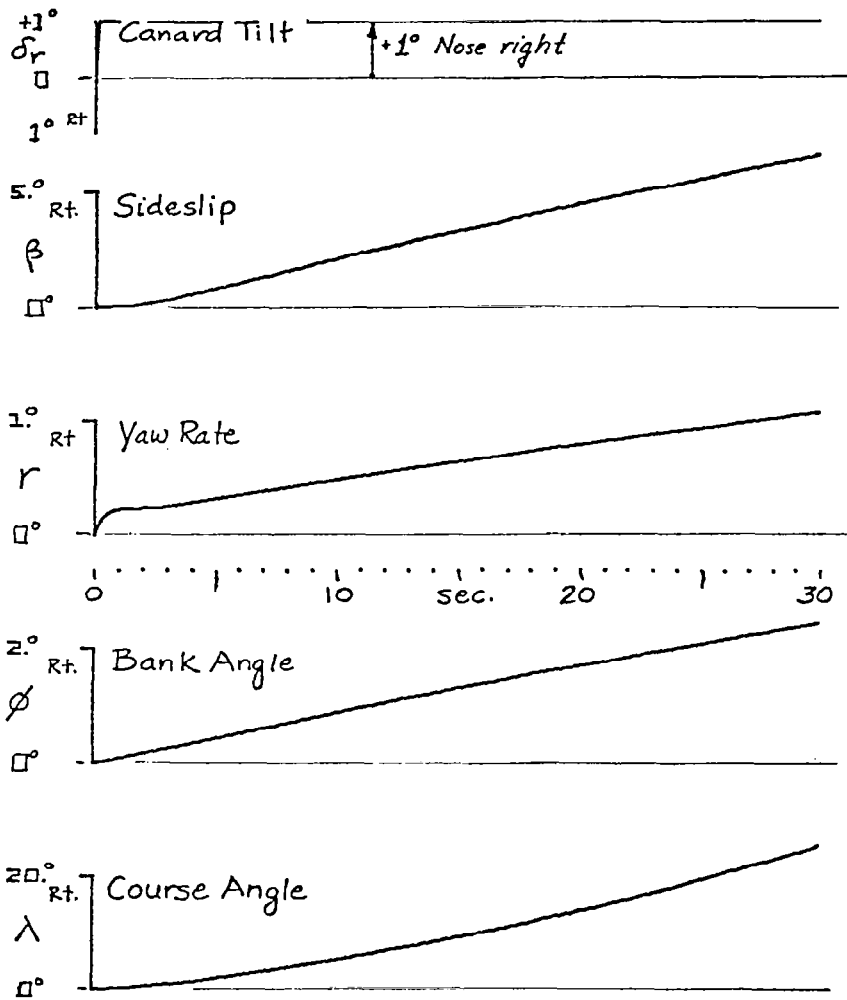


Figure A-2. Transient Response of Gossamer Condor to a Rightward Canard Tilt.

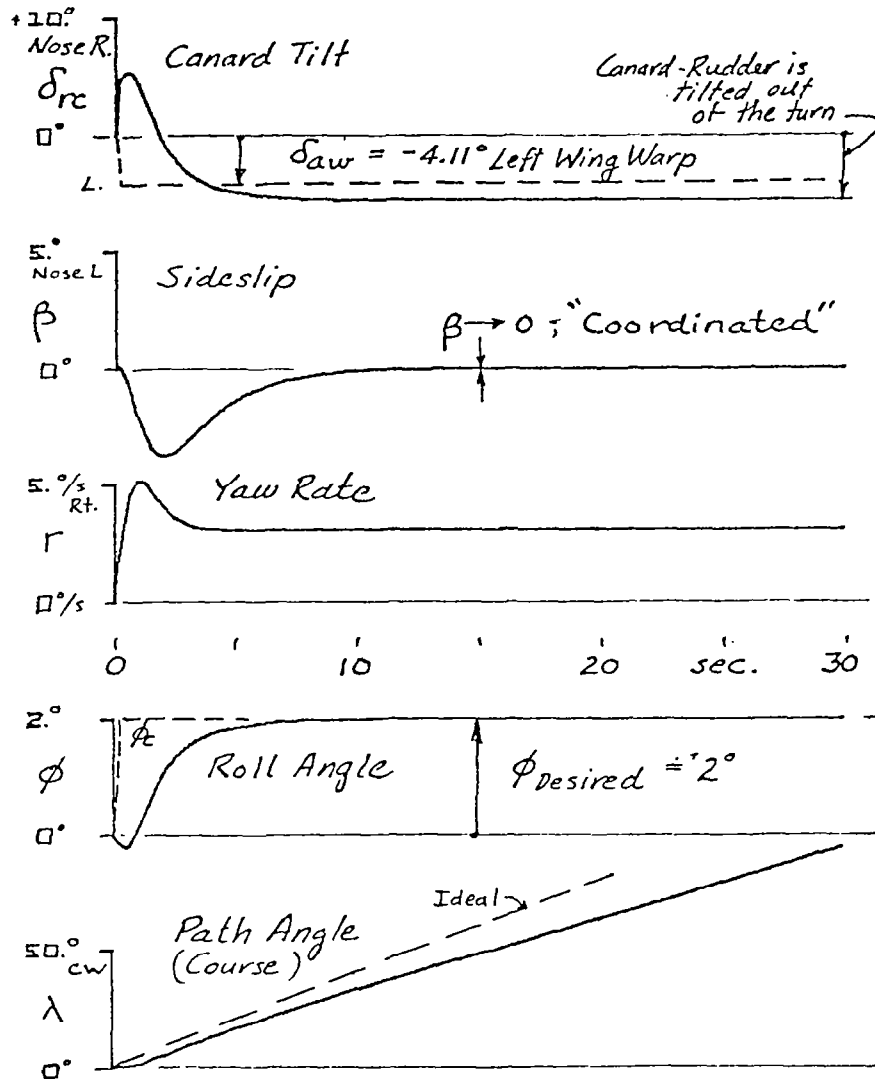


Figure A-3. Time Response of a Closed-Loop Turn Entry for the Gossamer Condor.

1. Report No. NASA CR-3627	2. Government Accession No.	3. Recipient's Catalog No.	
4. Title and Subtitle STABILITY AND CONTROL OF THE GOSSAMER HUMAN-POWERED AIRCRAFT BY ANALYSIS AND FLIGHT TEST		5. Report Date October 1982	6. Performing Organization Code
		8. Performing Organization Report No. STI TR 2109-1 AV R 82/520	
7. Author(s) Henry R. Jex and David G. Mitchell		10. Work Unit No. H-1178	11. Contract or Grant No. NAS4-2705
9. Performing Organization Name and Address Systems Technology, Inc. 13766 South Hawthorne Boulevard Hawthorne, California 90250		13. Type of Report and Period Covered Contractor Report—Final	
		14. Sponsoring Agency Code RTOP 505-41-14	
12. Sponsoring Agency Name and Address National Aeronautics and Space Administration Washington, D.C. 20546		15. Supplementary Notes Performed under subcontract P.O. 49526 from AeroVironment, Inc., Pasadena, CA 91107. Formerly published as NASA CR-163119. NASA Technical Monitor: R. Dale Reed, Ames Research Center, Dryden Flight Research Facility.	
16. Abstract <p>The Gossamer series of human-powered aircraft—the Gossamer Condor, first to fly the Kremer Figure-8 course, and the Gossamer Albatross, first to cross the English Channel—incorporated unconventional features such as: canard (tail first) configurations, pusher propellers, and wire-braced wings. They used wing warp for roll trim, and a tilting canard surface for pitch and yaw control. Their slow flight speed, very light wing loading and neutral stability emphasized "apparent-mass" aerodynamic effects and unusual modes of motion response. These are analyzed, approximated, and discussed, and the resulting transfer functions and dynamic properties are summarized and compared.</p> <p>To verify these analytical models, flight tests were conducted at the NASA Dryden Flight Research Facility with an electrically-powered Gossamer Albatross II. Sensors were installed for: control surface deflections, three-axis angular rates, three-axis accelerations, angle of attack, sideslip, airspeed, altitude, propeller speed, and power. Their outputs were telemetered to recorders on the ground. Frequency sweeps of the various controls were made and the data were reduced to frequency domain measures. Results are given for the responses of: pitch rate, airspeed and normal acceleration from canard-elevator deflection; roll rate and yaw rate from canard-rudder tilt; and roll rate and yaw rate from wing warp. The reliable data are compared with the analytical predictions, showing good agreement in longitudinal responses and fair agreement in lateral-directional responses.</p> <p>Areas deserving further research are identified as: unsteady aerodynamic effects, aeroelastic effects, gust response aerodynamics and pusher-propeller characteristics.</p>			
17. Key Words (Suggested by Author(s)) Stability and control, Flight dynamics, Flying qualities, Ultralight aircraft, Human-powered aircraft, Aircraft performance, Flight control system, Flight test techniques		18. Distribution Statement Unclassified—Unlimited STAR category: 02	
19. Security Classif. (of this report) Unclassified	20. Security Classif. (of this page) Unclassified	21. No. of Pages 80	22. Price* A05

*For sale by the National Technical Information Service, Springfield, VA 22161

NASA-Langley, 1982